

195
6-4-82
②

PPPL-1894
UC20-F

I-3536 ①

Lh. 590
PPPL-1894


A DENSITY-RISE EXPERIMENT ON PLI

MASTER

by

J.D. Strachan, N. Bretz, E. Mazzucato, C.W. Barnes,
D. Boyd, S. Cohen, J. Hovey, R. Kaita, S.S. Medley,
G. Schmidt, G. Tait, and D. Voss

May 1982

**PLASMA
PHYSICS
LABORATORY** 

**PRINCETON UNIVERSITY
PRINCETON, NEW JERSEY**

PREPARED FOR THE U.S. DEPARTMENT OF ENERGY,
UNDER CONTRACT DE-AC02-76-CNO-3073.

IF THIS DOCUMENT IS UNLAWFUL

A DENSITY-RISE EXPERIMENT ON PLT

J.D. Strachan, N. Bretz, E. Mazzucato, C.W. Barnes,⁽¹⁾
D. Boyd,⁽²⁾ S. Cohen, J. Hovey, R. Kaita, S.S. Medley,
G. Schmidt, J. Tait, and D. Voss⁽³⁾

Plasma Physics Laboratory
Princeton, New Jersey 08544

PPPL--1894
DE82 015484

ABSTRACT

The evolution of the density profile in PLT during intense gas puffing is documented and analyzed. Measurements of the spectrum of low energy edge neutrals and of the change in central neutral density indicate that charge-exchange processes alone cannot account for the central density rise. The transient density profile changes can be reproduced numerically by a diffusivity of $\sim 10^4$ cm²/s, and a spatially averaged inward flow of 10^3 cm/s. These transport coefficients are $10 + 10^2$ times larger than neoclassical. The ion energy confinement is reduced, the small scale density fluctuations are increased, and runaway electron losses are increased during the density rise.

(1) Los Alamos National Laboratory
CTR-5, Ms-302
Los Alamos, NM 87545

(2) Dept. of Physics and Astronomy
University of Maryland
College Park, MD 20742

(3) Lawrence Livermore National Laboratory
L-45, P.O. 808
Livermore, CA 94550

DISCLAIMER

This document contains information which is being furnished by an agency of the United States Government to the recipient for his own use, and is not to be distributed outside the agency. The views and opinions of the recipient are not to be construed as those of the United States Government. The views and opinions of the recipient are not to be construed as those of the United States Government or any agency thereof.

DISTRIBUTION OF THIS DOCUMENT IS UNLIMITED

Introduction

Plasma densities have been raised by gas puffing in a number of tokamak experiments.¹⁻⁶ In the smaller devices, the evolution of the density profile can be explained by assuming an edge neutral temperature of 10-50 eV. This allows edge neutrals to penetrate deeply into the plasma before being ionized. However, for larger devices such as PLT or at the higher densities found in Alcator, the mean-free-path for edge neutral penetration becomes much smaller than the minor radius. Nevertheless, in PLT and Alcator the electron density profiles have remained parabolic as was observed in the smaller devices. Previously, the density rise was modeled^{6,7} with neoclassical transport modified by an increased edge neutral energy caused, for example, by neutral interactions at the limiter, and by a modestly enhanced (2 to 3 times) Ware pinch. Such small deviations from neoclassical transport cannot explain the rapid changes in density reported here.

Gas can be puffed rapidly into PLT, doubling the density in 50-100 ms, but causing only small deviations from parabolic density profiles. However, due to the short mean-free-path, charge exchange cannot be an important transport process in the interior of PLT. In fact, without an anomalous transport mechanism, the edge density will rise rapidly, further shielding the center from edge neutrals. Therefore, experimental determination of the rate of central density increases and of the resulting density profiles, indicates a deviation from neoclassical transport. It is this deviation and its consequences which are described in the present paper.

The approach in this work has been primarily empirical. It was found that the central density rise comes from the puffing gas and not from a pinching of the initial plasma particles. A charge-exchange mechanism can be excluded since the central neutral density does not change during the gas

puffing. The outflux of low energy neutral particles was measured near and away from the limiter. Although the increase in recycling near the limiter is considerable, no increase is observed in the outflux of higher energy (300-1000 eV) edge neutrals at either location. These observations limit the models which can be used to explain the particle balance. If a simple one-dimensional transport model is assumed,⁸ the observation of parabolic density profiles implied the density rise is due to both an inward flow velocity which is about 10^3 cm/s near the edge decreasing to $\sim 10^2$ cm/s near the center, and a diffusion coefficient of $\sim 10^4$ cm²/s. These values are 10 to 10^2 times larger than neoclassical, and for the flow velocity, the radial dependence is opposite to that of the Ware pinch. However, in order to make the ion energy balance consistent with the inferred particle flows, either the ion heat conduction must be enhanced 6-7 times during the density rise, or the inward transport has to involve primarily colder particles.

To help identify possible mechanisms responsible for the transport, spatially resolved measurements of the density fluctuation spectrum have been made with 2 mm microwaves. During the rise, the magnitude of the fluctuations is observed to increase substantially.

When density rises, the ion confinement time decreases. However, despite the anomalies in the particle balance, following the density rise, both the electron and the ion confinement increase and become comparable to the highest PLT values.

Experiment

The PLT devices⁹ were operated, unless otherwise noted, with top-bottom carbon limiters, $a = 40$ cm, $R = 135$ cm, $B = 25$ kOe, $I = 400$ kA, and titanium gettered walls. The physical locations of the relevant diagnostics are shown

in Fig. 1. The gas injection valve is near the limiter. Its injection rate is controlled by a feedback system, in which the difference between the measured line-average density and its programmed evolution determines the voltage on a piezoelectric valve.¹² The response of the total system, including the gas valve conductance, is < 5 ms.

The density was increased from $\bar{n}_e \approx 2 \times 10^{13} \text{ cm}^{-3}$ to $4 \times 10^{13} \text{ cm}^{-3}$ in about 100 ms (Fig. 2a). The density profile determined from Thomson scattering remained centrally peaked during the gas puffing (Fig. 3a and 3c). The density profiles have a systematic asymmetry caused by a slight misalignment between the Thomson scattering laser and the spectrometer.¹¹ The data shown in Fig. 3c is uncorrected for this and the 3-D plot averages the profiles about the center. The central density is delayed with respect to the line-averaged value ($1.5 \times \bar{n}_e$) by 10-20 ms. The density evolution is reproducible, as are the current and voltage waveforms. However, there are occasional changes in the MHD activity in the equilibrium before the density rise. Before the rise, sawtooth oscillations are not observed often, but during and after the rise, they almost always occur.

When the initial plasma and puffing gas are both deuterium, the neutron emission falls during the density rise (Fig. 4), but the emission rises afterward to a level which is ten times higher. The ion temperature deduced from the charge-exchange spectrum and from neutron emission falls about 100 eV during the rise but returns thereafter to its initial level (Fig. 2b).

The plasma current rises at a small rate throughout the discharge (0.2 kA/ms). The loop voltage rises somewhat during the density rise and thereafter falls to about 1 volt/turn. The peak electron temperature is shown in Fig. 2b from the $2\omega_{ce}$ emission. The increase in T_e just before the density rise occurs at the beginning of the sawtooth MHD activity. Some differences

between the emission and Thomson scattering measurements may be due to the fact that the emission resolution is about 10 cm vertical and about 3 cm horizontal, while the Thomson scattering¹¹ profiles are measured along a vertical chord at $R = 134$ cm, with a vertical resolution of 3 cm and a horizontal resolution of 3 mm. The profiles of Fig. 3 were made up of 24 Thomson scattering profiles measured at 10 times during the discharges and thus form a multiple shot composite of the plasma evolution.

The role of impurities in the power balance is relatively small. The total radiated power profile measured by the bolometer array (Fig. 1) is relatively flat. The central value is ~ 30 mW/cm³ rising to ~ 50 mW/cm³ between 30 and 40 cm. Thus the radiated loss in the central region is $< 10\%$ of the 400-500 mW/cm³ ohmic power input, and the radiated power equals the ohmic input only in the outer regions ($r > 30$ cm). The influence of the density rise is to temporarily increase the edge radiation by $\sim 30\%$. The initial plasma has $Z_{\text{eff}} = 1.5-2$ from the resistivity, and $Z_{\text{eff}} = 2.0-3.0$ spectroscopically. After the density increase, Z_{eff} drops to 1.0 (resistivity) - 1.5 (spectroscopic). Thus the influx of gas does not bring in new impurities. The edge radiation from CII, H β , and similar lines do increase by factors of 3-20 during the gas puff; however, immediately after the rise in density, the line intensities revert to their previous levels.^{6,10} A more complete account of the spectroscopic measurements in this type of discharge can be found in Reference 12.

The data shown in Figs. 2 and 3 refer to an initial deuterium plasma with a deuterium gas puff. In order to determine the rate at which the puffing gas arrives in the center, two similar auxiliary experiments have been carried out. We have puffed hydrogen into a deuterium plasma and deuterium into a hydrogen plasma. The evolution of the measured parameters is nearly identical

to that described for the deuterium into deuterium case. The neutron emission for the pure deuterium and for deuterium puffed into an initial hydrogen plasma is shown in Fig. 4. The expected centrally peaked profile of the ion temperature ensures that all the neutrons come from $r/a \leq 1/4$; thus the ion temperature dependence can be unfolded from the emission rate yielding the time evolution of the central deuterium density. The result for deuterium into hydrogen is shown in Fig. 5. The central density rise can be entirely accounted for by particles puffed from the gas valve, since the increase in neutron emission can be accounted for by the deuterium reaching the plasma center. When hydrogen is puffed into an initially deuterium discharge, the neutron emission remains relatively constant. The central deuterium density (Fig. 6) also remains relatively constant, indicating that there is no substantial change in the amount of initial plasma gas recycled at the plasma edge and, as in the previous case, there is no large expulsion or concentration of the original discharge gas during the density rise.

The uncertainty in the central ion temperature evolution makes these determinations somewhat uncertain since the neutron emission depends roughly on $n_e^2 T_i^4$. It should be noted from Fig. 4 that deuterium puffing into a hydrogen plasma immediately caused the neutron emission to rise in spite of the falling ion temperature. This implies that immediate penetration of the puffing gas by a transport process must be taking place, since multiple charge exchange would not allow penetration of the injected gas.

The evolution of the central neutral density has been deduced from the energetic charge-exchange outflux at two toroidal locations. The magnitude of the neutral outflux is corrected for the time evolution of the ion temperature and the fractional escape of the neutrals out of the plasma. Well away from the limiter ($\sim 110^\circ$ toroidally - Fig. 1), the central neutral density falls by

a factor of two, but near the gas inlet ($\sim 10^\circ$ toroidally-Fig. 1) and limiter ($\sim 15^\circ$), the central neutral density remains relatively constant (Fig. 7) during the rise. We conclude from these measurements that the rise in central density cannot be accounted for by ionization of neutrals at the center.

The outflux of low energy (50-1000 eV) neutrals from the periphery of the discharge has been measured by a time-of-flight spectrometer¹³ and by deuterium depth implantation in carbon probes¹⁴ (Fig. 1). Away from the limiter and gas valve the outflux of neutrals with energies ≥ 50 eV decreases during the gas puff by a factor of two, and the average energy decreases by 30%. The outflux near the limiter is simulated at this toroidal location by inserting an auxiliary carbon button limiter from the top of the vessel at the neutral spectrometer port (Fig. 1). This limiter was adjusted to receive about 20% of the power deposited on the main limiter. With the button limiter inserted, the average neutral flux was 10-50 times higher, and the time evolution during the gas puff was relatively constant. The lower energy flux increased (Fig. 8a), while the higher energy flux (Fig. 8b) decreased. The shape of the low energy spectrum reveals that the edge ion temperature decreases from 45 (± 10) eV to 20 (± 10) eV.

The absolute magnitude and shape of the measured neutral outflux spectrum was used to estimate the absolute values of the edge and central neutral densities at the limiter. The estimate is based upon calculation of the expected neutral emission¹³ using the measured $T_e(r)$, $n_e(r)$, $T_1(o)$ and the edge neutral temperature as a variable parameter. Before the gas puffing (300 msec in Fig. 8), the edge neutral density $n_o(a) \sim 2 \times 10^9 \text{ cm}^{-3}$ and the central neutral density $n_o(o) \approx 1 \times 10^8 \text{ cm}^{-3}$, while at the end of the gas puff (475 msec), $n_o(a) \approx 7 \times 10^9 \text{ cm}^{-3}$ and $n_o(o) \approx 5 \times 10^7 \text{ cm}^{-3}$. The values of n_o away from the main and the auxiliary limiters are estimated to be about 7

times lower. The uncertainties in these values due to the absolute calibration and the plasma opacity is about a factor of two.

The neutral particle data imply that the energetic deuterium source function at the edge of the plasma does not change substantially when the density increases due to the gas puff. Furthermore, the decrease in higher energy flux allows less neutral particle penetration through the plasma boundary. As a result, one expects that the density increase must be explained ultimately by plasma transport processes.

Energy Confinement Time

The central electron power balance ($r \leq 15$ cm) is shown in Fig. 9. The input power from ohmic heating is balanced primarily by electron conduction before the density rise, but afterwards, 25-50% of the input is lost to the ions. The uncertainty in the central power input is due to an uncertainty in the current distribution. During the density rise, the profile changes are rapid enough that it is necessary to calculate the internal fields using the magnetic diffusion equation:

$$\frac{\partial}{\partial r} \left[\frac{n}{r} \frac{\partial (rB_{\theta})}{\partial r} \right] + \frac{4\pi}{c} \frac{\partial B_{\theta}}{\partial t} = 0 . \quad (1)$$

The resistivity, η , is a function of the measured electron temperature and (more weakly) of B_{θ} through the trapped particle correction. The current and loop voltage are used to calculate $Z_{\text{eff}}(t)$ self-consistently from the temperature measurements. If the radial profile of Z is assumed constant, $q(0) \approx 0.7$ after the density rise. A central accumulation of impurities, or

the absence of any trapped particle correction to the resistivity, can raise the estimate of $q(0)$ to 0.9-1.0. However, the central power input is uncertain only to about 20% because a lower current density is roughly compensated by an increased resistivity. Usually, $q(0)$ is thought to be ~ 1.0 , especially with the presence of sawtooth MHD activity.

The central electron energy confinement time, τ_{Ee} , can be calculated from the time evolution of the electron energy content, E_e :

$$\tau_{Ee}(15 \text{ cm}, t) = \frac{\int_0^{15 \text{ cm}} E_e r dr}{\int_0^{15 \text{ cm}} (P_{OH} - P_{ei} - dE_e/dt) r dr} \quad (2)$$

The initial value of τ_{Ee} shown in Fig. 10 is about 35 ms, which is typical of PLT confinement times at this density.¹⁵ The electron confinement time stays relatively constant through the density rise, but it increases to 60 ms at the density maximum primarily because the loop voltage falls and the power transferred to the ion goes up, leaving less power to be lost through the electron channel.

The ion energy content triples as a result of the density rise. The empirical ion energy flow (Fig. 11) indicates that an increase occurs in the power input from electron-ion collisions (P_{ei}). If the measurement uncertainty in both T_e and T_i are taken into account, the error in P_{ei} after the rise is considerable. However, we take the upper boundary of the P_{ei} estimate to obtain the lower bound on the ion energy confinement time, τ_{Ei} , for $r \leq 15 \text{ cm}$ as shown in Fig. 10.

$$\tau_{Ei} (15 \text{ cm}, t) = \frac{\int_0^{15\text{cm}} E_i r dr}{\int_0^{15\text{cm}} (P_{ei} - dE_i/dt) r dr} \quad (3)$$

The ion confinement time value begins at about 60 ms, decreases during the gas puff as P_{ei} increases, but rises back to its previous level after the density increase has stopped.

The total energy confinement time

$$\tau_E = \frac{\int_0^a (E_e + E_i) r dr}{\int_0^a [P_{OH} - \frac{d}{dt} (E_e + E_i)] r dr}, \quad (4)$$

is dominated by the electrons, but rises to 80-90 ms at 600-650 ms in the discharge (Fig. 12). This value is close to the highest attained in PLT.¹⁰

Particle Balance

The electron density ($n_e = n_i = n$) is presumed to change in time due to diffusion by either neoclassical (D^{NC}) or anomalous (D^A) processes, to directed convection by either neoclassical (Ware drifts, V^W) or anomalous (V^A) processes, and to ionization of neutrals by electron impact ionization ($\langle \sigma v \rangle_{ei}$).

$$\frac{\partial n}{\partial t} = \frac{1}{r} \frac{\partial}{\partial r} [r (D^{NC} + D^A) \frac{\partial n}{\partial r}] + \frac{1}{r} \frac{\partial}{\partial r} [r n (V^W + V^A)] + n n_0 \langle \sigma v \rangle_{ei} \quad (5)$$

The neoclassical coefficients for the Ware pinch velocity (Fig. 13a) and the diffusion coefficient⁷ (Fig. 13b) have rather small numerical values for PLT.⁵ Neoclassical theory is unable to describe the experimental density rise. Thus, the experimental evolution of the plasma density profile is used to yield information on the anomalous coefficients. The calculation of the neutral density and the temperature are difficult to determine experimentally.

The one-dimensional diffusion equation (Eq. 5) was solved by the Crank-Nicholson implicit difference method. The spatial diffusion was averaged in time. The edge neutral density and edge neutral temperature are considered input variables. The consequence of a purely neoclassical calculation for the experimental PLT parameters is that the density profile becomes hollow (Fig. 14), contrary to the experimental observations. Increasing the neutral penetration by changing the edge neutral energy to 500 eV during the gas puff still results in a hollow density profile. The basic problem is that the neutral gas penetration is unstable to the hollowing of the density profile (i.e., building up the edge density) during intense gas puffing. Once the edge density begins to flatten, there is less neutral penetration, resulting in a faster buildup of edge density and so on. Another way of expressing this problem is that the combined action of the neoclassical inward velocity and the neoclassical diffusion coefficient is insufficient to transport particles away from the edge region, where they build up due to the ionization of the neutrals whose densities have been increased by the gas puffing. A comparison of the neoclassical terms which contribute to the change in particle density is shown in Fig. 15.

An arbitrary increase ($\times 10$) in the pinch velocity, keeping the diffusion neoclassical, can increase the central density at the experimentally observed rate (Fig. 16). However, the density profile becomes more peaked inside

FIGURE CAPTIONS

Schematic diagram of PLT indicating the toroidal location of the

$r = 15$ cm than is observed, and the $10\times$ neoclassical pinch cannot prevent the profile from hollowing at the edge.

Pure neoclassical calculations are unable to account for the experimentally observed density rise in PLT, even with a $5 + 10 \times$ enhanced edge neutral temperature and/or a $10\times$ enhanced Ware pinch. At the minimum, the transport processes nearer the plasma periphery ($r > 25$ cm) need to be enhanced over neoclassical. The anomalous diffusion coefficient and anomalous inward directed velocity in Eq. (5) are used to estimate the magnitude of the anomalous transport processes. If the anomalous processes dominate the entire particle balance, then the typical steady-state parabolic density profiles provide a specific relationship between the anomalous inward directed velocity and the anomalous diffusion⁸

$$v^A(r) = \dots \frac{2rD^A}{a^2 - r^2} = \frac{D^A}{n} \frac{\partial n}{\partial r} \quad \left| \text{parabolic } n \text{ profiles.} \right. \quad (6)$$

Following Coppi,⁸ the steady-state plasma convection is modeled as a competition between a radially-independent diffusion process (Fig. 13b) and an inward directed velocity (Fig. 13a), which is larger toward the plasma periphery in such a manner that the two processes balance when the profile is parabolic. This means that a slight flattening of the density will allow the inward velocity term to dominate the diffusion, tending to restore the parabolic profile.

Calculations with this type of anomalous process indicate that a diffusion coefficient of about 10^4 cm²/sec (to within about a factor of three) is required to explain the PLT gas puff experiments. Most of the density

increase is due to the anomalous inward velocity, while the large diffusion coefficient is required for a quick relaxation back to a near parabolic profile (Fig. 17). The anomalous contributions to the change in density are shown in Fig. 18

Calculations with only a large anomalous diffusion coefficient which is independent of r and no large inward directed velocity also do not explain the FLT results. The equilibrium profiles themselves tend to be flat and the density tends to become hollow during the density rise.

Ion Energy Balance

Since the particle balance is anomalous, with inward and outward fluxes exceeding the net particle flux by about a factor of ten, it is interesting to examine the neoclassical ion energy balance for the discharges in Figs. 2 and 3. The ion energy flow (dE_i/dt) is balanced according to

$$\frac{dE_i}{dt} = P_{ei} + P_{tc} + P_{pc} + P_{cx} - P_{iz} , \quad (7)$$

where the electron ion coupling (P_{ei}), the neoclassical thermal conduction (P_{tc}), the charge-exchange losses (P_{cx}), and the reionization energy gain (P_{iz}) are defined in Ref. 16.

$$P_{pc} = \frac{1}{r} \frac{\partial}{\partial r} \left[r \frac{3}{2} kT_i \Gamma \right] + \frac{nk_i}{r} \frac{\partial}{\partial r} (r \Gamma/n) , \quad (8)$$

and uses the net particle flux, Γ , which is determined through the particle balance equation:

$$\frac{\partial n}{\partial t} = \frac{1}{r} \frac{\partial}{\partial r} (r\Gamma) + nn_0 \langle \sigma v \rangle_{ei} . \quad (9)$$

The ion temperature evolution is modeled by assuming a steady state at 300 ms and taking experimental values for $T_e(r,t)$, $n_e(r,t)$, and Z_{eff} . The value $q(0,t) = 1.0$ was arbitrarily fixed during the rise and $B_\theta(r,t)$ was determined by assuming the current profile is proportional to $T_e^{3/2}$. The results discussed here are relatively insensitive to the form of $q(r)$. Relative to the diffusion calculation discussed earlier, the neoclassical heat conduction coefficient¹⁶ ($\propto q^2$) may be slightly overestimated for $r \lesssim 10$ cm and slightly underestimated over the outer portion of the discharge. We have also taken a toroidally averaged $n_0(r=0) = 10^8 \text{ cm}^{-3}$ initially. Any value larger than this would be inconsistent with the initial ion energy balance and is somewhat higher (5x) than is expected from the low energy neutral data. The profile of n_0 and T_0 are calculated from a short mean-free-path model from Ref. 17. The time evolution of $n_0(r=0)$ is taken from the experimental data.

The calculation shows that before and after the density rise the heat loss can be explained mainly by neoclassical heat conduction to the boundary. However, during the rise the inward flow of heat from convection and electron-ion coupling is not balanced by neoclassical conduction and, as a result, the model predicts an increase in the ion temperature instead of the observed decrease. Figure 19 shows the predicted neutron flux compared to the

experimental value. The calculation can be made to agree with the experiment in several possible ways:

- (a) The heat conduction can be increased during the density rise by a factor of 6-7.
- (b) The central neutral particle density can be increased by a factor of ~ 10 (in contradiction to our charge-exchange measurements, which show the central density to be constant or decreasing).
- (c) The net particle influx brings little energy into the plasma center. That is, the anomalous convection process brings particles but little energy into the center as if the convection were an energy dependent process.

Of these possibilities, (b) can be excluded by the measurements and particle balance modelling, but we cannot distinguish, so far, between (a) and (c), either of which is possible.

Fluctuations

The small-scale electron density fluctuations measured in PLT by scattering of microwaves^{18,19} were observed to change during the rapid rise of the plasma density. An array of antennae, located in the same poloidal plane, was used for launching the output of a 140 GHz extended interaction oscillator and for collecting the waves scattered by fluctuations of the plasma density. Spatial resolution was obtained by using high gain antennae (≈ 38 db). The typical scattering region had a length of about 10 cm in the radial direction. The k -resolution ($\approx \pm 1 \text{ cm}^{-1}$) was determined by the finite dimensions of the scattering volumes.

The differential cross section for incoherent scattering of electromagnetic waves by electron density fluctuations is

$$\sigma = \sigma_0 S(\vec{k}, \omega),$$

where $\sigma_0 = (e^2/mc^2)^2$ is the Thomson cross section and $S(\vec{k}, \omega)$ is the spectral density of electron fluctuations. The frequency ω and the wave vector \vec{k} must satisfy the energy and momentum conservation, i.e., $\omega = \omega_s - \omega_i$ and $\vec{k} = \vec{k}_s - \vec{k}_i$, where the subscripts s and i refer to the scattered and the incident wave respectively.

Shown in the insert in Fig. 20 is the typical frequency spectrum of fluctuations with $k = 7 \text{ cm}^{-1}$ during the stationary phase of a discharge with $\bar{n}_e = 1.3 \times 10^{13} \text{ cm}^{-3}$. The spectrum is shifted towards the negative frequency side which, for this particular scattering geometry, is that of waves with phase velocities along the electron diamagnetic velocity. From these measurements we estimate that the quantity $\langle |u|^2 \rangle / \langle n \rangle$ has a value of $\approx (0.5-1.0) \times 10^{-2}$ in the central region of the discharge ($r \approx 0 - 15 \text{ cm}$) and a value of $\approx (2-4) \times 10^{-2}$ in the outer region ($r \approx 30-40 \text{ cm}$).

The time evolution of density fluctuations at two radial locations is shown in Fig. 20 for a discharge where the average density was raised from $1.4 \times 10^{13} \text{ cm}^{-3}$ to $2.8 \times 10^{13} \text{ cm}^{-3}$ in about 40 msec. Shown in Fig. 20 is the quantity

$$\left[\int_{-\infty}^{+\infty} S(k, \omega) d\omega \right]^{1/2}.$$

From these data, one can see that at the edge of the plasma column the level of fluctuations starts to increase as soon as the density begins to rise, and it reaches a maximum after 20 msec. At the same time, in the central region of the plasma column, the turbulence at first decreases to a minimum, and then it returns to its original value. At this moment, the amplitude of fluctuations starts to increase rapidly throughout the plasma column, and it reaches a maximum at the end of the density rise. The ratio of the peak over the initial amplitude is about a factor of two in the central region and four in the outer region. The peak amplitude increases with the rate of rise of the density. The spectral shift towards the electron diamagnetic direction tends to increase in the outer region and to diminish in the center during the density rise.

As the plasma density stops rising, the turbulence decreases to a new stationary level which, with respect to the amplitude before the density rise, is almost unchanged in the central region, while it is about two times larger (or equal to the ratio of the density increase) in the outer region.

There is also a similarity between the time evolution of the density fluctuations and the hard X-ray emission caused by runaway electrons leaving the plasma and striking the limiter. On other PLT discharges,²⁰ the fluctuation spectrum of the hard X-ray signal was similar to the spectrum of the density fluctuations. During the density rise, the time evolution of both signals is similar (Fig. 2f), as is the time evolution of the low energy neutral outflux (Fig. 8a). The peak of the hard X-ray signal also increases with the rate of density rise. For the discharges used in the density rise experiments, the runaway electron levels were too low to obtain meaningful fluctuation spectra.

Increased Rate of Density Rise

When the rate of rise of the density is increased beyond that described in the previous section, the magnitude of the density fluctuations increases (Fig. 22), the dip in the neutron intensity (and thus T_i) is enhanced, the density profile flattens and the loop voltage increases (to 1.9 volts for $dn/dt \approx 7 \times 10^{14} \text{ cm}^{-3} \text{ sec}^{-1}$). The discharges tend to become irreproducible and disruptive when the rate of density rise is above $\dot{\bar{n}}_e = 5 \times 10^{14} \text{ cm}^{-3} \text{ sec}^{-1}$. The tendency toward disruptions is reduced if neutral beam heating is used during the density rise. Figure 23 shows a beam assisted density rise where the electron density is increased from $\bar{n}_e = 1.6 \times 10^{13} \text{ cm}^{-3}$ to $6 \times 10^{13} \text{ cm}^{-3}$ with $dn/dt = 2 \times 10^{15} \text{ cm}^{-3}/\text{s}$. Deuterium beams of 1.8 MW are used to maintain the plasma temperature - $T_e(0) \approx 1.3 \text{ keV}$, $T_i(0) \approx 2.0 \text{ keV}$. The initial plasma is deuterium, the puffing gas is helium in order to aid the neutral beam penetration, the toroidal field is 32 kG, and $I_\phi = 450 \text{ kA}$. The gas puffing is intense enough to form a hollow density profile with the maximum at $r = 20 \rightarrow 30 \text{ cm}$. The beam itself makes no appreciable contribution in the density rise either at the density maximum or at the plasma center (less than 10% is caused by beam particles).

One expectation is that the main influence of the neutral beam heating is to stabilize the electron temperature and current density profiles, which would otherwise undergo considerable redistribution due to the large influx of cold gas. These beam-assisted density rises provide further empirical evidence for the magnitude of the particle transport coefficients. The hollow density profile means that it is feasible for the central density to rise entirely by a diffusive process. Putting

$$\frac{\partial n}{\partial t} (r = 0) \approx D^A \frac{1}{r} \frac{\partial}{\partial r} \left(r \frac{\partial n}{\partial r} \right)$$

means that D^A is of the order of $5 \times 10^3 \text{ cm}^2/\text{sec}$ for it to account for the experimentally observed $\partial n/\partial r \sim 2 \times 10^{15} \text{ cm}^{-3} \text{ sec}^{-1}$ with the experimentally observed $\partial n/\partial r \sim 10^{12} \text{ cm}^{-2}$. The anomalous coefficients used earlier (Fig. 13) can also reproduce the experimentally observed profiles (Fig. 23) where now the diffusive term (D^A) dominates the directed velocity term (v^A) due to the inverted profile.

Another beam assisted density rise case provides further empirical evidence for the magnitude of the directed velocity term (v^A) (Fig. 24). Now $\frac{\dot{n}}{n_e}$ of $\sim 10^{15} \text{ cm}^{-3} \text{ sec}^{-1}$ was obtained with 1.5 MW of deuterium beam heating of a hydrogen plasma, and the density profile was flat throughout the steepest part of the density rise (Fig. 24). In this case $\partial n/\partial r = 0$, so that diffusive terms (even if D is a function of minor radius) are less important. Putting

$$\frac{\partial n}{\partial t} (r = 0) = \frac{1}{r} \frac{\partial}{\partial r} r n v^A$$

means that a spatially averaged velocity v^A is of the order of $10^3 \text{ cm}/\text{sec}$. Again modelling this density rise with both anomalous coefficients (Fig. 13) reproduces the experimentally observed profiles, and the directed velocity term does dominate inside $r \sim 30 \text{ cm}$.

The fact that the density profiles do not change appreciably until the rate of density rise becomes $\sim 10^{15} \text{ cm}^{-3} \text{ sec}^{-1}$ and only becomes hollow for $\frac{\dot{n}}{n_e} \sim 2 \times 10^{15} \text{ cm}^{-3} \text{ sec}^{-1}$, empirically indicates that the particle influx rate is larger than the outflux due to transport. For the lower rates of density rise of $\frac{\dot{n}}{n_e} = 2 \times 10^{14} \text{ cm}^{-3} \text{ sec}^{-1}$ of Figs. 2 and 3, the profiles were not highly perturbed since the transport processes were much larger than the particle influx rate (Fig. 18).

Discussion

The evolution of the density profile during gas puffing experiments on PLT indicates that particle transport could be due to the combination of an inwardly directed velocity ($v^A \sim 10^3$ cm/sec) that is peaked towards the plasma periphery, and a large anomalous diffusion coefficient ($D^A \sim 10^4$ cm²/sec), as has been suggested previously on the basis of Alcator gas puffing experiments.⁸ This experimental conclusion is derived from PLT plasma conditions where the density rises strongly and the plasma is evolving in time. However, these transport coefficients for the hydrogen ions also would explain PLT transport measurements of trace high Z impurities²¹ and trace ³He ions²² which were performed in quasi-steady-state plasma conditions. The results reported here cannot be explained by enhanced neutral penetration, coupled with a mildly enhanced Ware pinch, and which has previously been used to explain PLT and Alcator density profiles.⁷ The enhanced Ware pinch leads to more peaked profiles rather than slightly broader profiles. Enhanced neutral penetration, as might be caused by an increased edge neutral temperature, leads to hollow density profiles. Charge-exchange measurements of the central neutral density evolution and the neutral emission from the limiter indicate that neutral particle penetration did not cause the density rise. Since an inwardly directed velocity is necessary to model the experimental results, it is worth considering possible mechanisms for the generation of this inward drift.

Although the results reported here do not directly contradict an inwardly directed velocity produced by modes driven by electron temperature gradient, ²³ $v \propto \partial T_e / \partial r$, earlier PLT results with hollow electron temperature profiles had centrally peaked density profiles instead of the hollow density profiles expected if the pinch were driven by electron temperature gradients.²⁴

The pinch velocity (Fig. 13) has roughly the same radial profile as the neutral density, since both terms fall one to two orders of magnitude from the plasma periphery to the plasma center. The pinch velocity is approximately $\sim 10\rho_i/\tau_{CX} \sim \rho_0/\tau_{CX}$ when averaged over the plasma, and it is $\sim \rho_i/\tau_{CX}$ near the limiter and gas inlet where ρ is the Larmor radius and τ_{CX} is the charge-exchange time. Thus, mechanisms are possible which involve displacement of ions by the charge-exchange process. Also, it is expected that the cold gas will perturb the plasma column in the vicinity of the gas inlet and the limiter. This perturbation should have a radial profile similar to the neutral density profile; thus, mechanisms are possible which involve electric fields set up by three dimensional asymmetries.

Perhaps there is a connection between the inward flow and microturbulence. The pinch velocity (Fig. 13) has roughly the same radial profile as the density fluctuations in PLT,²⁵ since both fall one to two orders of magnitude from the plasma periphery to the plasma center. Moreover, the density rise and density profile evolution have a major influence on the magnitude of the density fluctuations. The pinch velocity of 10^3 cm sec⁻¹ with $\delta n/n$ of a few percent requires a specific phase relationship between poloidal electric and density perturbations such that the cosine of the phase is $\sim 0.1 \rightarrow 1$. Recent experiments on Macrotron²⁶ found potential and density fluctuations to be correlated, but the phase was not specified. The decrease of scattered amplitude at the end of the density rise is consistent with the observed improvement in energy confinement (Fig. 10).

Finally, we note that the evolution of the ion energy balance during the density rise indicates that, whereas the usual neoclassical analysis applies during the quasi-steady portions of the discharge, an anomaly exists during the density rise. The anomaly might be explained by a $5 \times$ enhanced ion

thermal conduction or an energy dependent convection process which brings little energy into the plasma center. There is a fundamental difficulty with the usual treatment of the convection term in the ion energy balance, since the inward and outward fluxes are much larger than the net flux of particles that is conventionally used to deduce the convective energy flow. This means that more energy can be transported by convection port processes. We note that differences in energy confinement between different tokamaks, and in heating quality between different experiments, may originate with the convection processes since such differences are often accompanied by density profile changes^{27,10} and particle recycling changes.

Acknowledgments

The authors thank W. Stodiek, J. Hosea and the PLT experimental group, as well as H. Eubank and the PLT neutral beam group for their help in performing these experiments. Helpful discussions with A. Boozer and W. Tang are also gratefully acknowledged. This work was supported by the U.S. Department of Energy Contract No. DE-AC02-76-CHO-3073.

REFERENCES

- ¹J.C. Hosea, C. Bobeldijk, and D.J. Grove, Plasma Physics and Controlled Nuclear Fusion Research (Proc. Int. Conf. 1971) paper IAEA-CN-28/F-7.
- ²O. Klüber, W. Englehardt, B. Cannici, J. Gernhardt, E. Glock, F. Karger, G. Lisitano, H.M. Mayer, D. Miesel, P. Morandi, S. Sesnic, J. Stadlbauer, F. Wagner, Nucl Fusion 15, (1975) 1194.
- ³K. Toi, S. Itoh, K. Kadota, K. Hawahata, N. Noda, K. Sakurai, K. Sato, S. Tanahashi, and S. Kasue, Nucl. Fusion 19, (1979) 1643.
- ⁴E. Apgar, B. Coppi, A. Gondhalekar, H. Helava, D. Komm, F. Martin, B. Montgomery, D. Pappas, R. Parker, D. Overskei, Plasma Physics and Controlled Nuclear Fusion Research (Proc. 6th Int. Conf., Berchtesgaden 1976) paper IAEA-CN-35/A5.
- ⁵V.V. Buzankin, V.A. Vershkov, Yu. N. Dvestrovtsij, A.B. Izvozchikow, E.A. Mikhajlov, and G.V. Pereverzev, Plasma Physics and Controlled Nuclear Fusion Research (Proc. 7th Int. Conf., Innsbruck, 1978) paper IAEA-CN-37/N-5-1.
- ⁶G.L. Schmidt, N.L. Bretz, R.J. Hawryluk, J.C. Hosea, and D.W. Johnson in Proc. of 1st Fusion Funding Workshop (U.S. DOE, Washington, D.C., 1978) p. 53.
- ⁷M.H. Hughes, PPPL-1411 (1978).
- ⁸B. Coppi, Comments on Plasma Physics and Controlled Fusion, 5, 2C1 (1980).
- ⁹D. Grove, V. Arunasalam, K. Bol, D. Boyd, N. Bretz, et al., in Plasma Physics and Controlled Nuclear Fusion Research (Proc. of 6th Conf. Berchtesgaden, 1976) Vol I, p. 21.
- ¹⁰R. Hawryluk, K. Bol, N. Bretz, D. Dimock, D. Eames, et al., Nucl. Fus. 19, 1307 (1979).
- ¹¹N. Bretz, D. Dimock, V. Foote, D. Lang, E. Toluas, Ap. Optics 17 (1978) 192.
- ¹²E. Hinnov, J. Hosea, H. Hsuan, F. Jobs, E. Meservey, G. Schmidt, and S. Suckewer, Princeton University, Plasma Physics Laboratory Report, PPPL-1848 (1981) submitted to Nucl. Fusion.
- ¹³D.E. Voss and S.A. Cohen, J. Vac. Sci. and Tech. 17, (1980) 303.
- ¹⁴S.A. Cohen, H.F. Dylla, W.R. Wampler, C.W. Magee, J. Nucl. Mat. 93 & 94 (1980), 109.
- ¹⁵K. Bol, V. Arunasalam, M. Bitter, D. Boyd, K. Brau, et al., in Plasma Physics and Controlled Nuclear Fusion Research (Proc. 7th Int. Conf. Innsbruck, 1978) Vol 1, IAEA Vienna (1979) 11.
- ¹⁶M. Brusati, S.L. Davis, J.C. Hosea, J.D. Strachan, S. Suckewer, Nucl. Fus. 18, 1205 (1978).

- ¹⁷R.J. Goldston, Princeton University, Plasma Physics Laboratory Report, PPPL-1443 (1978).
- ¹⁸E. Mazzucato, Phys. Fluids 21, (1978) 1063.
- ¹⁹E. Mazzucato, Princeton University, Plasma Physics Laboratory Report, PPPL-1653 (1980).
- ²⁰C.W. Barnes, R.L. Dewar, E. Mazzucato, J.D. Strachan, Physics Letters 81A, 275 (1981).
- ²¹W. Stodiek, R. Goldston, N. Sauthoff, V. Arunasalam, C. Barnes et al., Vol. I, p. 9 (Brussels, 1980).
- ²²R. Chrien, H.P. Eubank, D.N. Meade, J.D. Strachan, Nucl. Fusion 21, (1981) 1661.
- ²³T. Antonsen, B. Coppi, R. Englade, Nuclear Fusion 19, (1979) 641. B. Coppi and N. Sharky, Nucl. Fusion 21, (1981) 1363. B. Coppi and C. Spight, Phys. Rev. Lett. 41.
- ²⁴A. Boozer - Private communication.
- ²⁵E. Mazzucato - unpublished.
- ²⁶S. Zweben and R.J. Taylor, Nucl. Fusion 21, (1981) 193.
- ²⁷R. Goldston, S. Davis, H. Eubank, R. Hawryluk, D. Johnson, et al., Second Joint Varenna - Grenoble International Symposium on Heating in Toroidal Plasmas, Como, 1981 - unpublished.

FIGURE CAPTIONS

1. Schematic diagram of PLT indicating the toroidal location of the relevant diagnostics and equipment: A - Limiters; B - Gas inlet, $2 \omega_{ce}$ polychrometer; C - Charge-exchange diagnostic; D - Microwave scattering; E - Thomson scattering; F - Low Energy Neutral analyzer, Movable limiter; G - Bolometer; H - Hard X-ray detector; I - Neutron detectors.
2. a) Time evolution of the loop voltage, V, the line average density \bar{n}_e , and the central electron density, $n_e(0)$ during the density rise.
b) Time evolution of the central electron temperature (-) from $2 \omega_{ce}$, and (●) from TVTS with the time evolution of the central ion temperature (--) from neutrons, and (x) from charge exchange during the density rise.
3. a) Evolution of the density profile as determined by the Thomson scattering.
b) $T_e(r)$ profiles at selected times in the density rise.
c) $n_e(r)$ profiles at selected times in the density rise.
4. Time evolution of the neutron emission during a deuterium gas puff into a deuterium plasma (I) and into a hydrogen plasma (Δ).
5. Central deuteron density during a deuterium gas puff in a hydrogen plasma. The error bars arise from counting statistics.
6. Central deuteron density during a hydrogen gas puff in a deuterium plasma. The error bars arise from counting statistics.
7. Relative time evolution of the central neutral density at a toroidal location near the limiter and gas inlet, as determined by the charge-exchange emission.
8. a) Neutral outflux at the movable limiter in the energy range 20-50 eV during an intense gas puff.
b) Neutral outflux at the movable limiter in the energy range 500 eV - 1 keV during an intense gas puff.
9. Central electron power flow ($r \leq 15$ cm) for the discharges of Figs. 2 and 3. P_{OH} is the ohmic power input, P_{ei} is the electron ion coupling.
10. Empirical electron and ion energy confinement times in the central plasma region ($r \leq 15$ cm).
11. Central ion power flow ($r \leq 15$ cm) for the discharges of Figs. 2 and 3.
12. Total energy confinement time for the discharges of Figs. 2 and 3.
13. a) Neoclassical and anomalous pinch velocities used in the particle balance.
b) Neoclassical and anomalous diffusion coefficients used in the particle balance.

14. Evolution of the density profile starting from an initial parabolic profile and evolving through a gas puff for the case of neoclassical transport coefficients.
15. Magnitude of the rate of density change caused by the neoclassical transport coefficients.
16. Evolution of the density profile starting from an initial parabolic profile and evolving through a 10X enhancement of the Ware pinch without an increase in the edge neutral density.
17. Evolution of the density profile starting from an initial parabolic profile and evolving through a gas puff using the anomalous transport coefficients of Fig. 13.
18. Magnitude of the rate of density caused by the anomalous transport coefficients.
19. Time evolution of the neutron emission $\{I\}$ for the discharges of Figs. 2 and 3. The solid line is the calculated neutron emission on the basis of the neoclassical ion energy balance.
20. Time evolution of the microwave signal scattered from small scale density fluctuations in the outer and central plasma regions. The insert shows a typical scattered spectrum which extends to 200 kHz.
21. Time evolution of the hard X-ray emission caused by runaway electron bombardment of the limiter.
22. Amplitude of the peak in the scattered microwave signal as a function of the rate of density rise.
23.
 - a) Time evolution of the density profile as determined by the Thomson scattering for a strong beam assisted density rise.
 - b) Time evolution of the central electron temperature.
 - c) $n_e(r)$ profiles at selected times in the beam assisted density rise.
24. Temperature and density profiles for a beam assisted density rise.

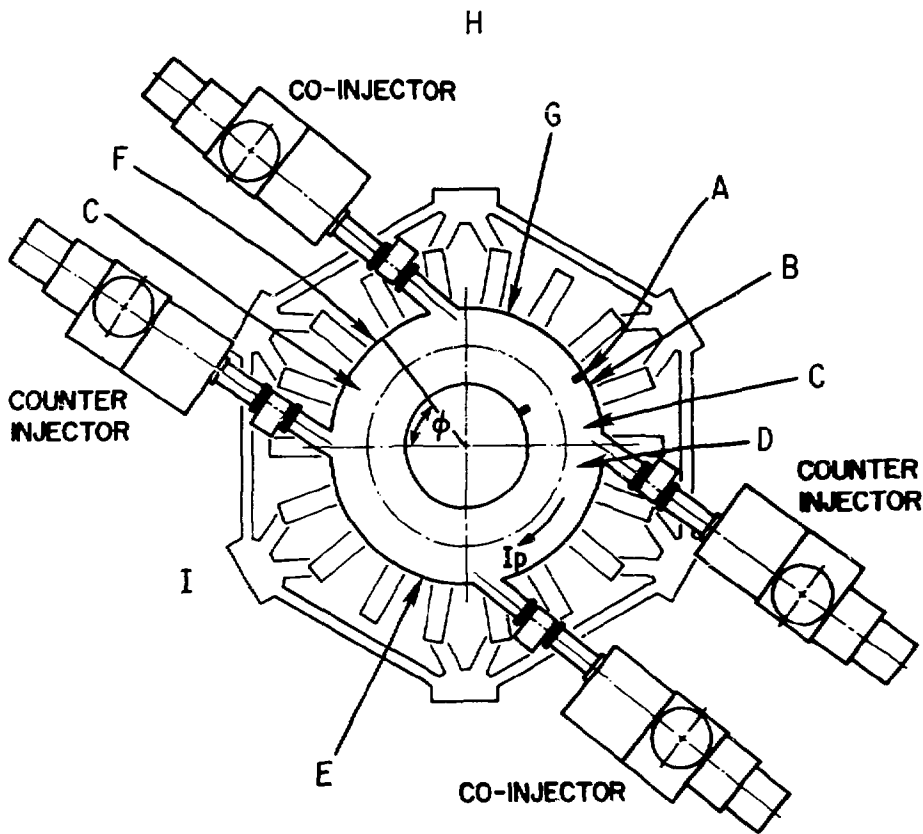


Fig. 1

#82 x 0200

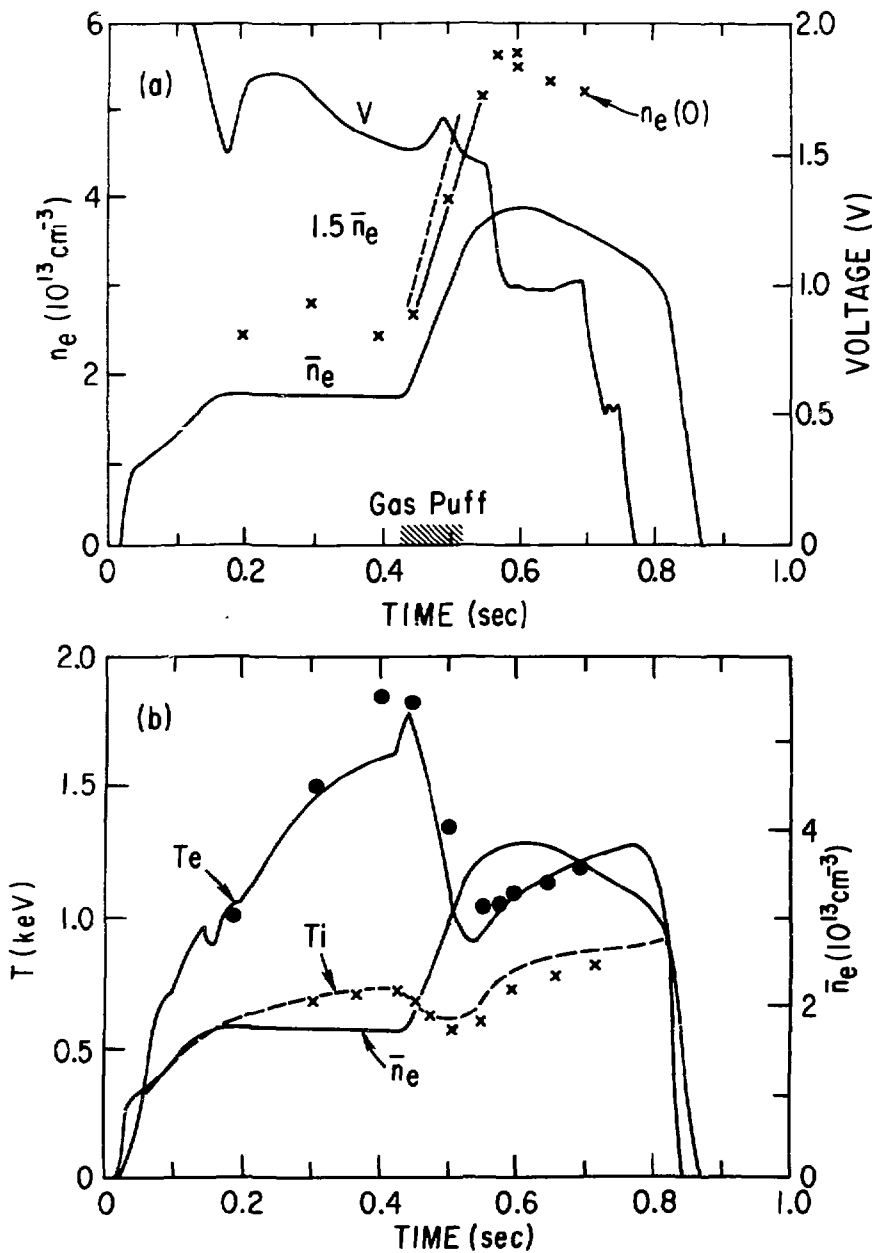


Fig. 2

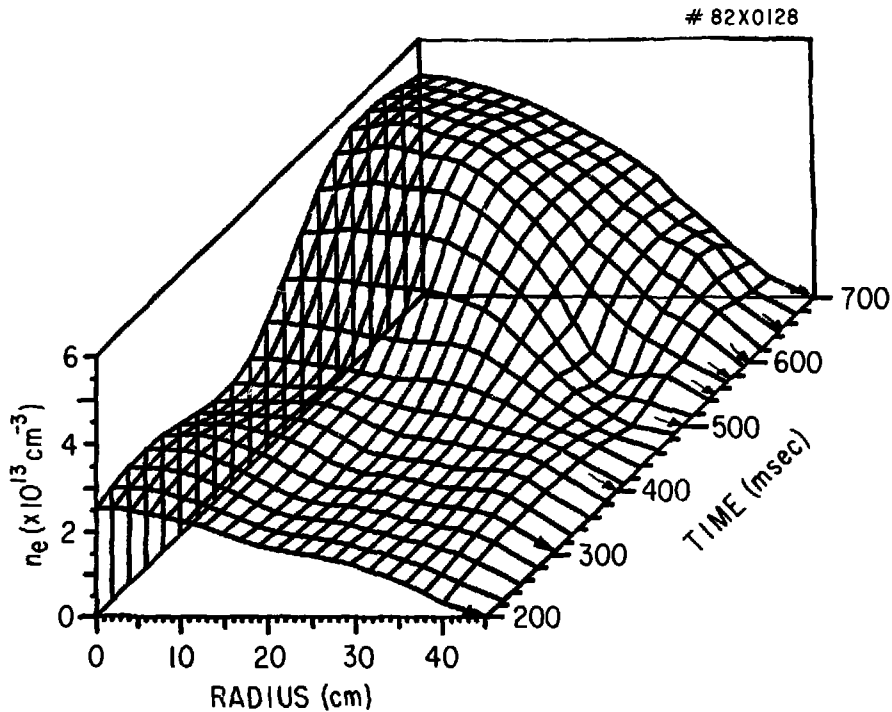


Fig. 3a

81 X 0176

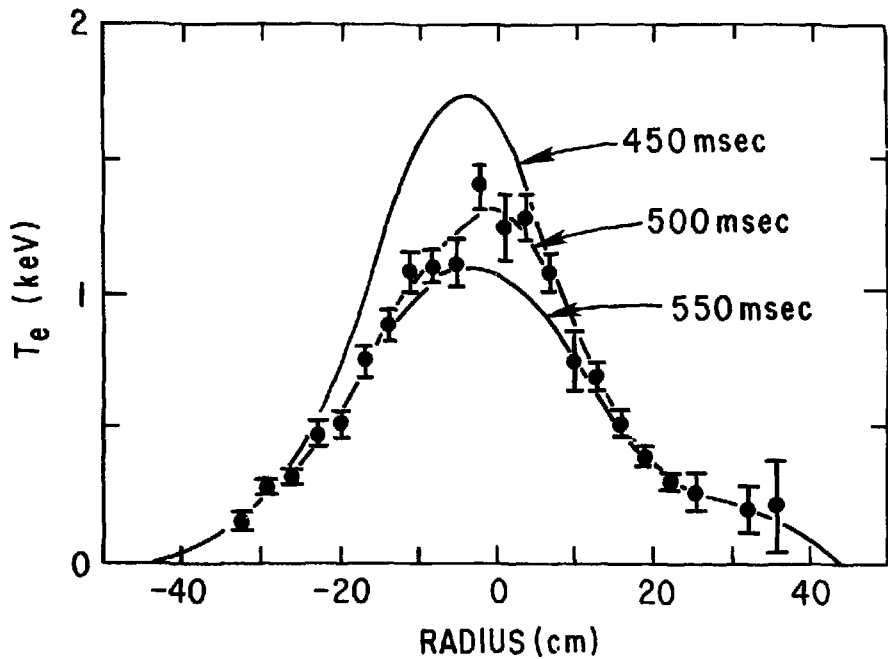


Fig. 3b

#81X0170

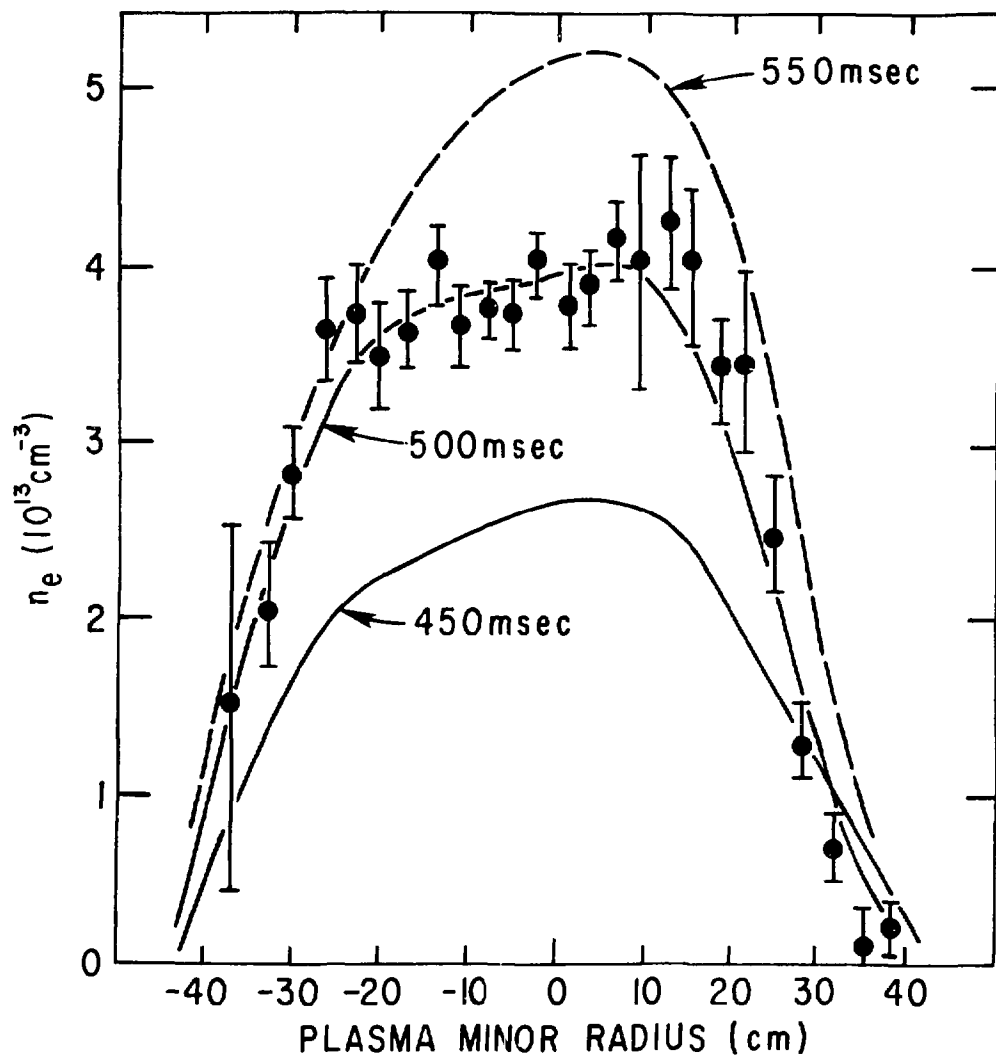


Fig. 3c

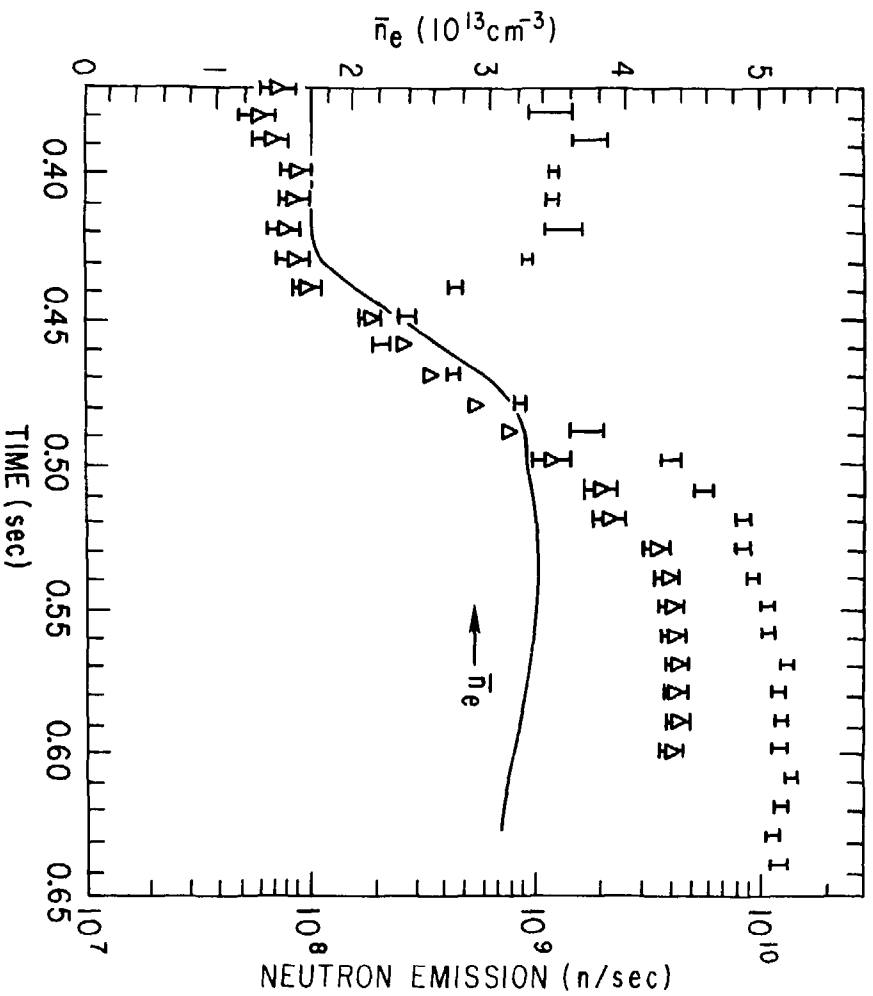


Fig. 4

#81X 0186

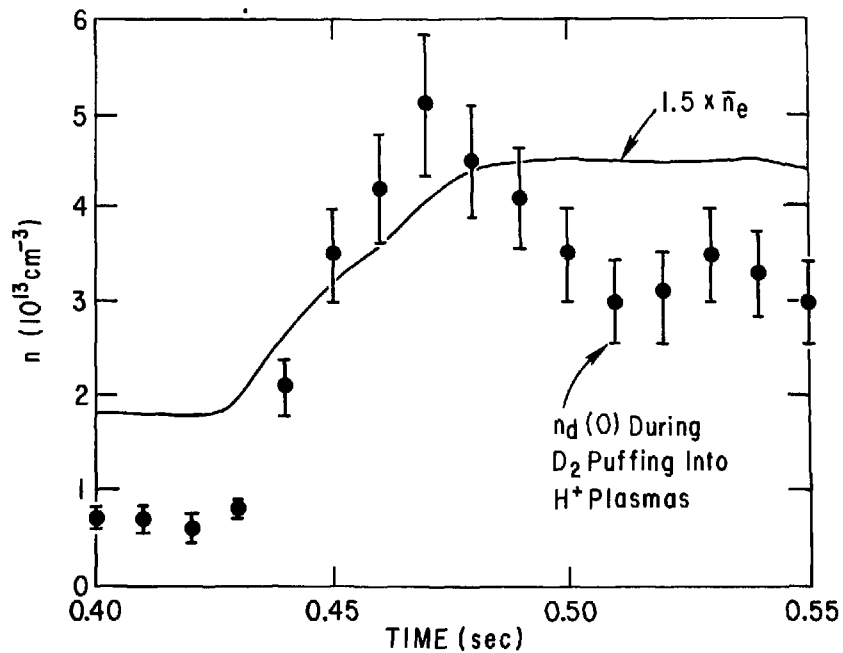


Fig. 5

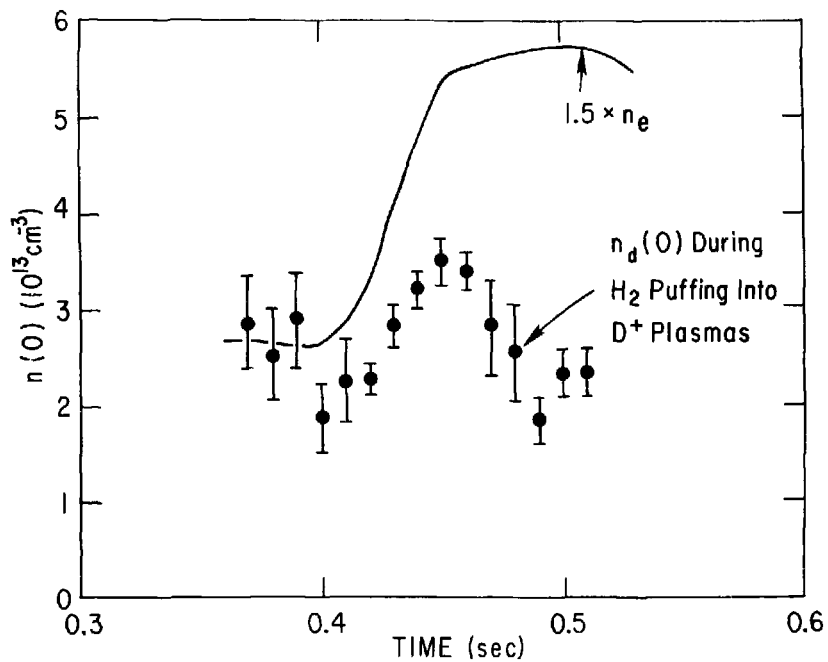


Fig. 6

81 X 0181

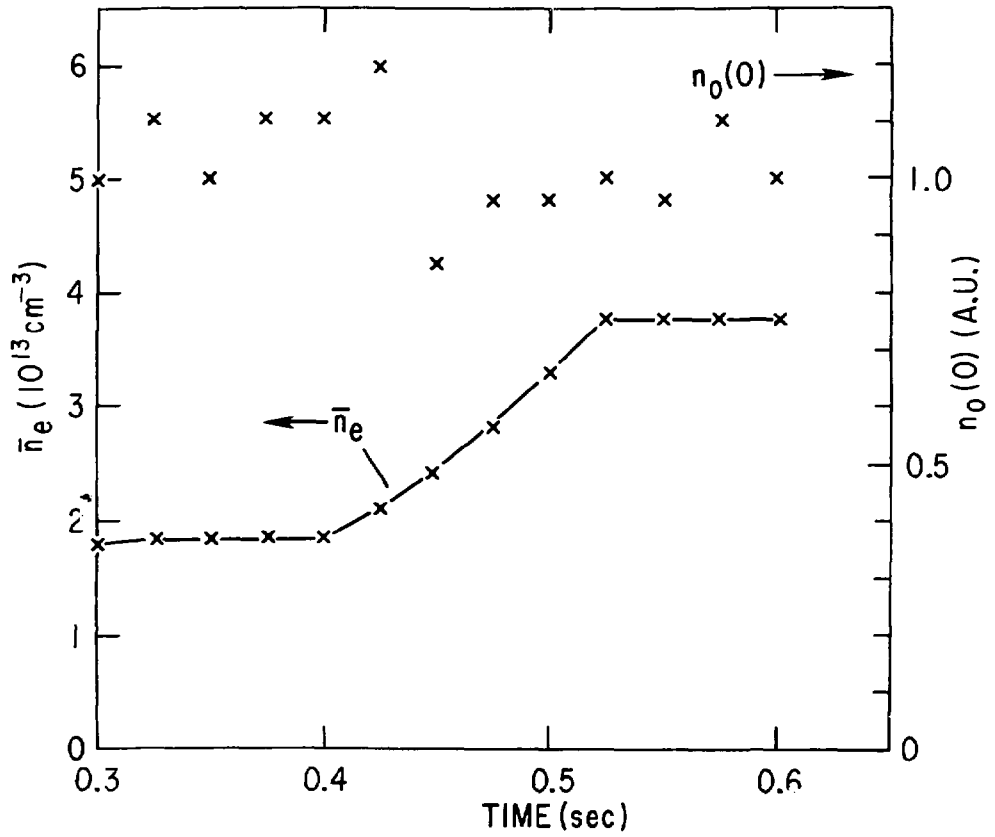


Fig. 7

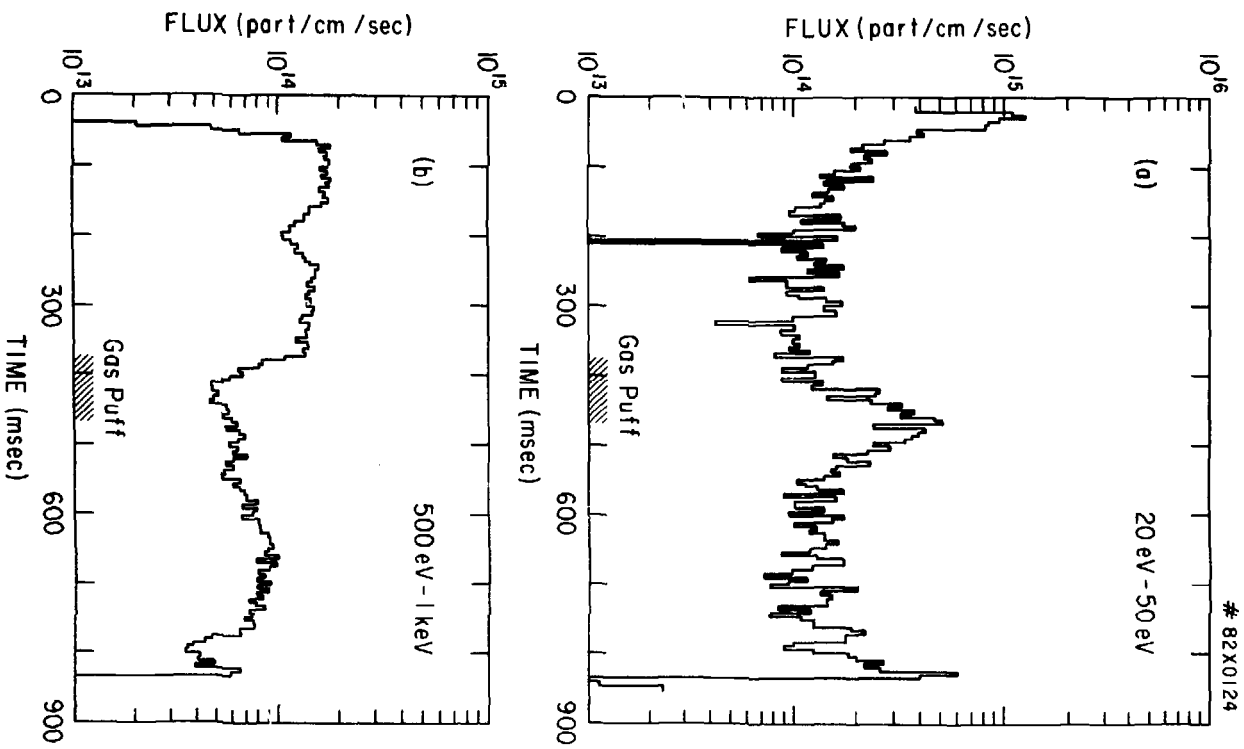


Fig. 8

82X0126

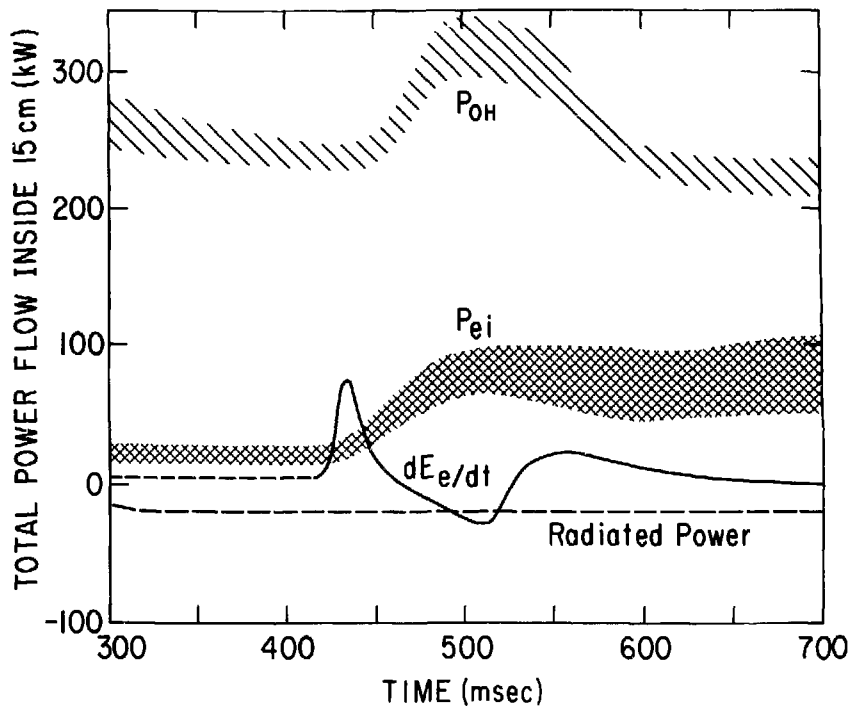


Fig. 9

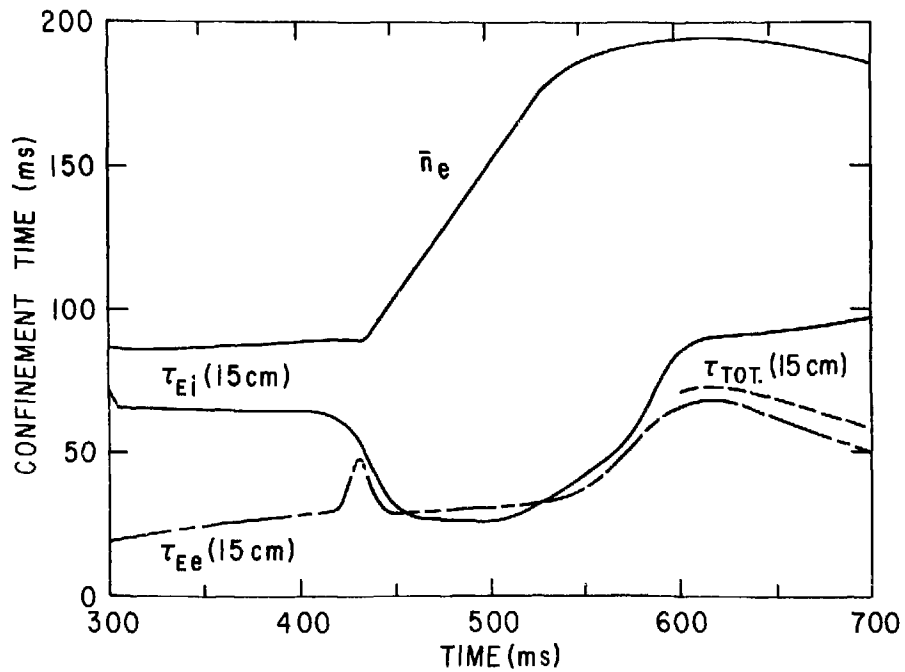


Fig. 10

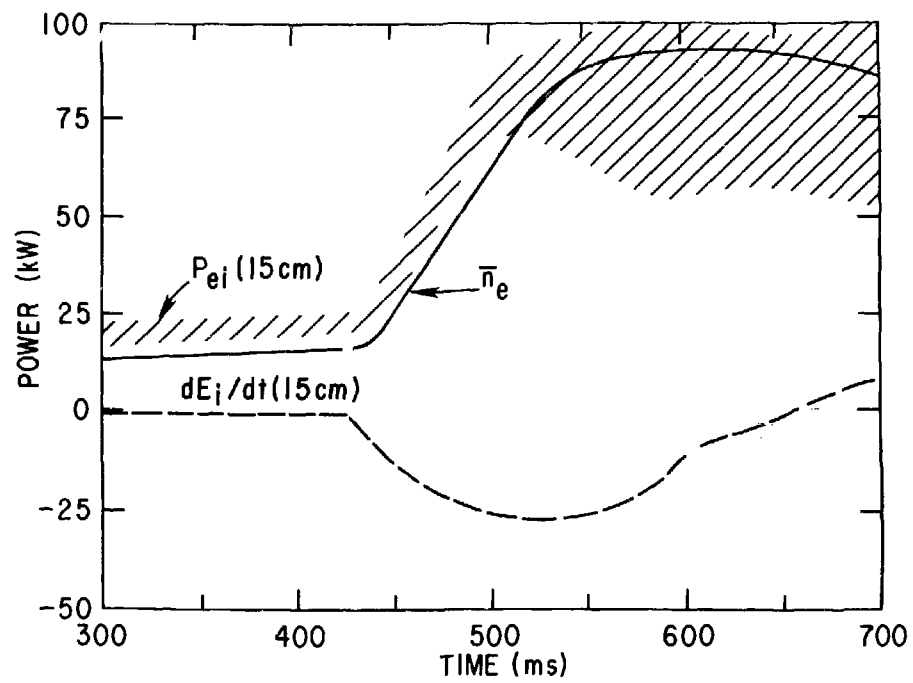


Fig. 11

#81X0187

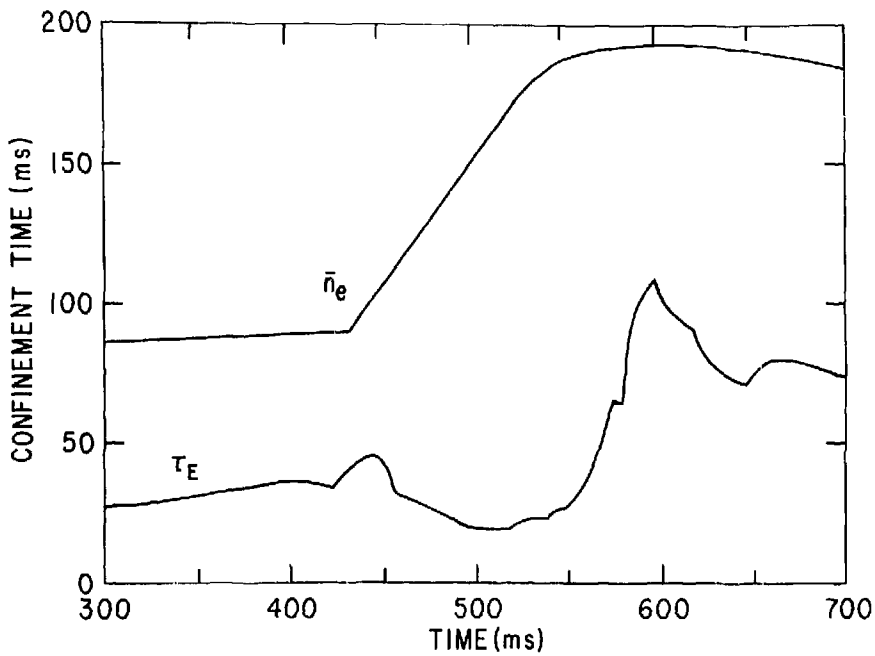


FIG. 12

81 X 0458

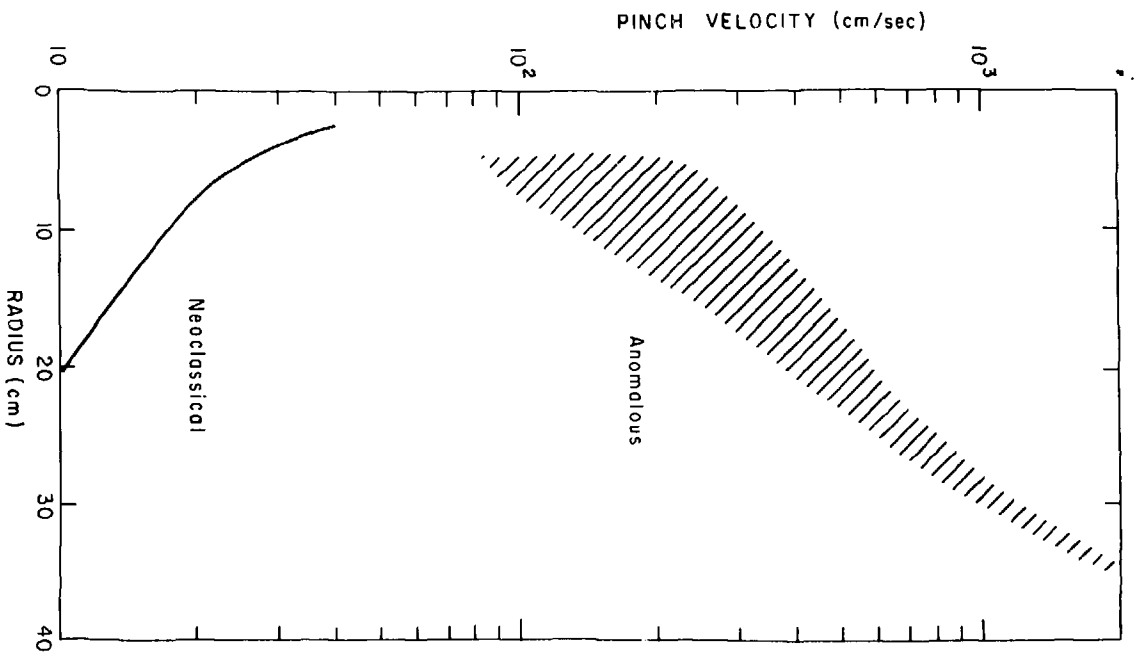


Fig. 13a

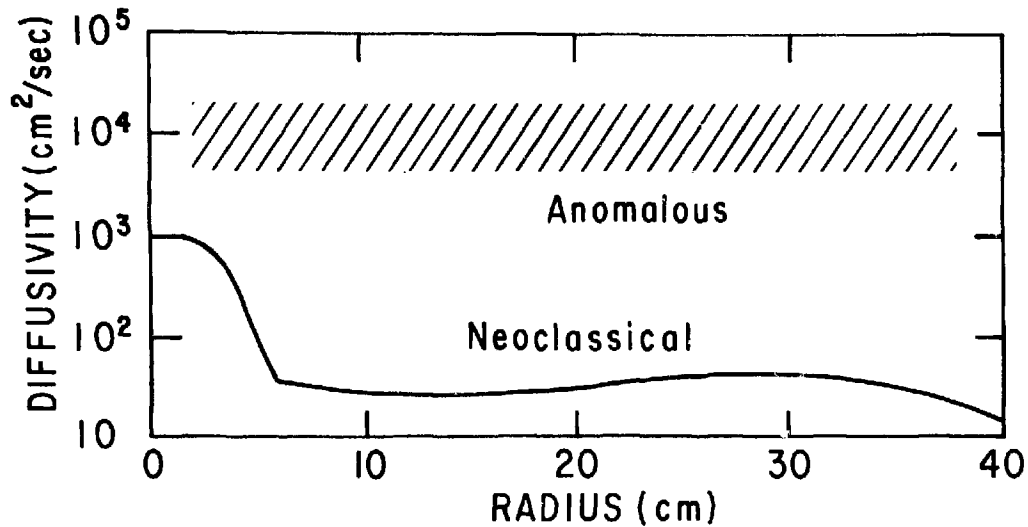
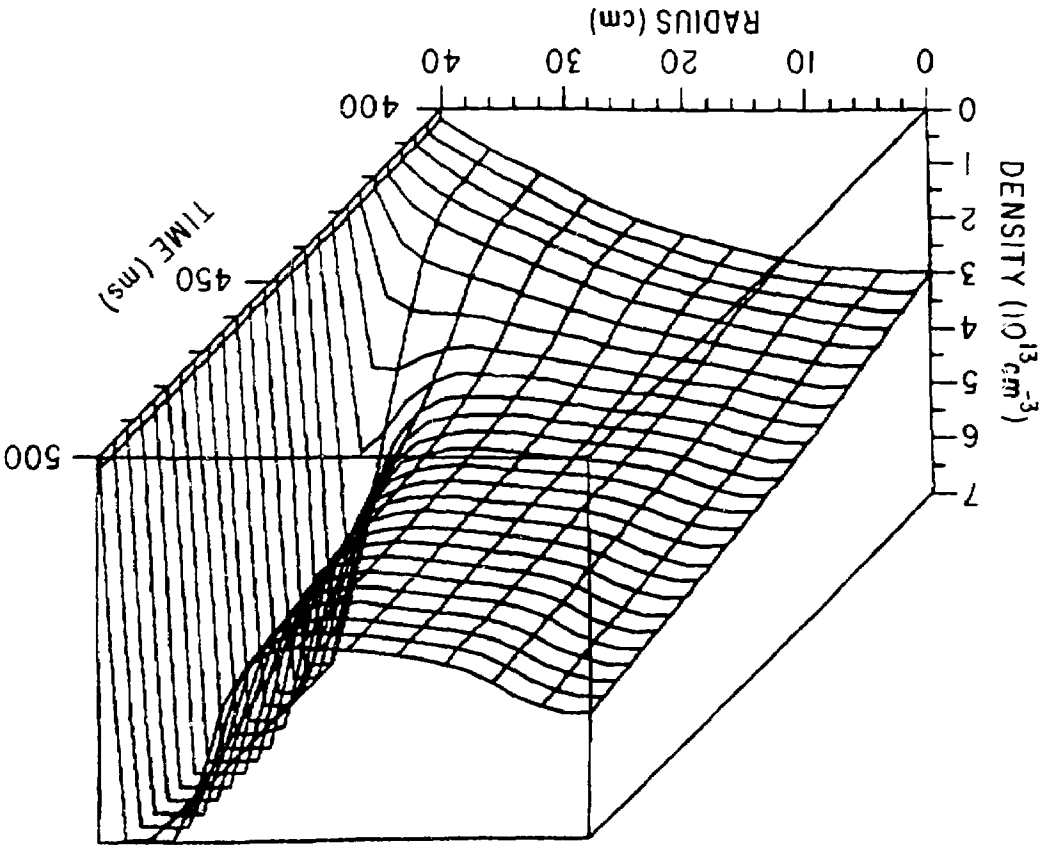


Fig. 13L

Fig. 14



#81X 0467

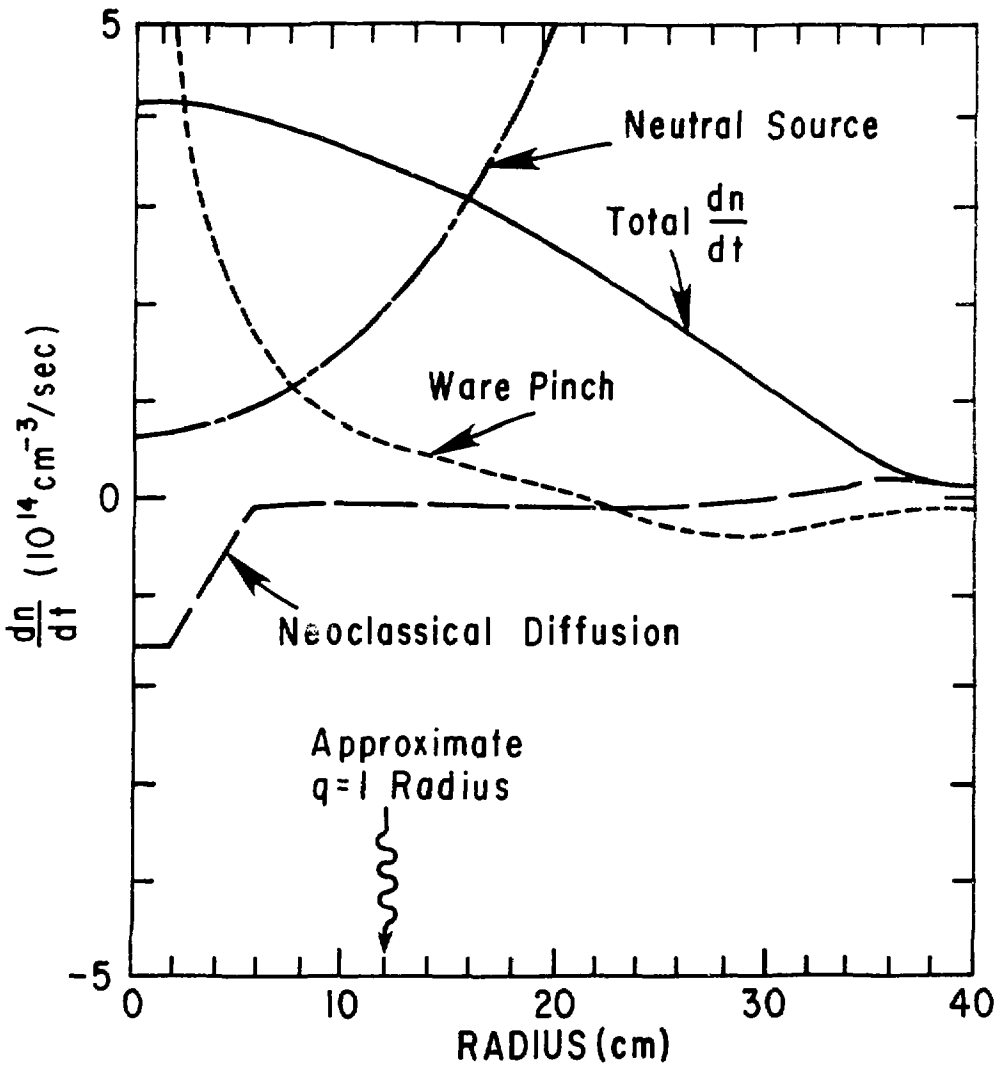


Fig. 15

81 X 0469

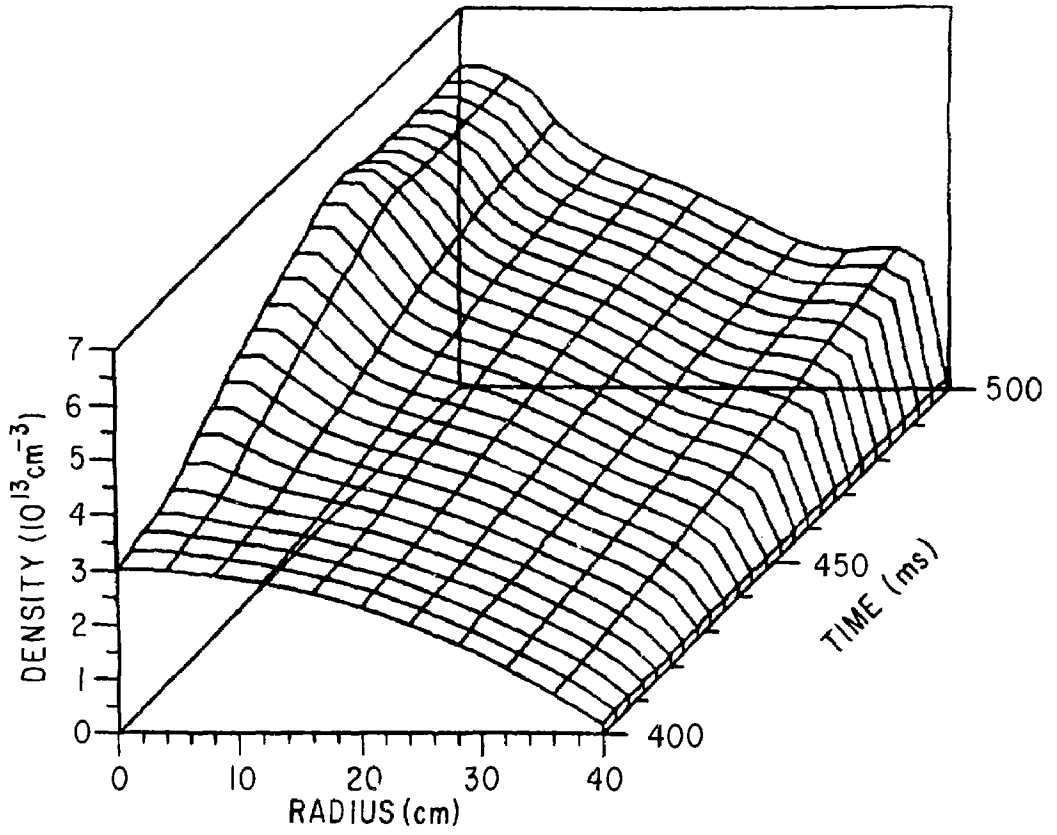


Fig. 16

#81X0471

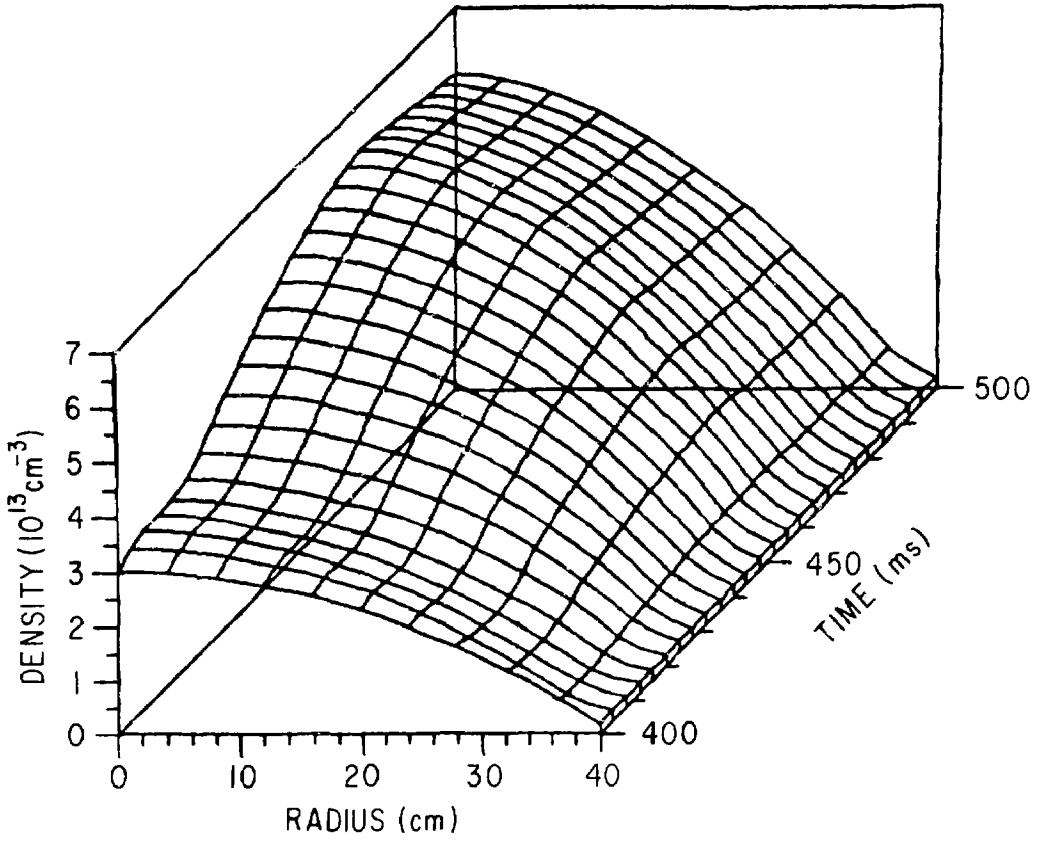


Fig. 17

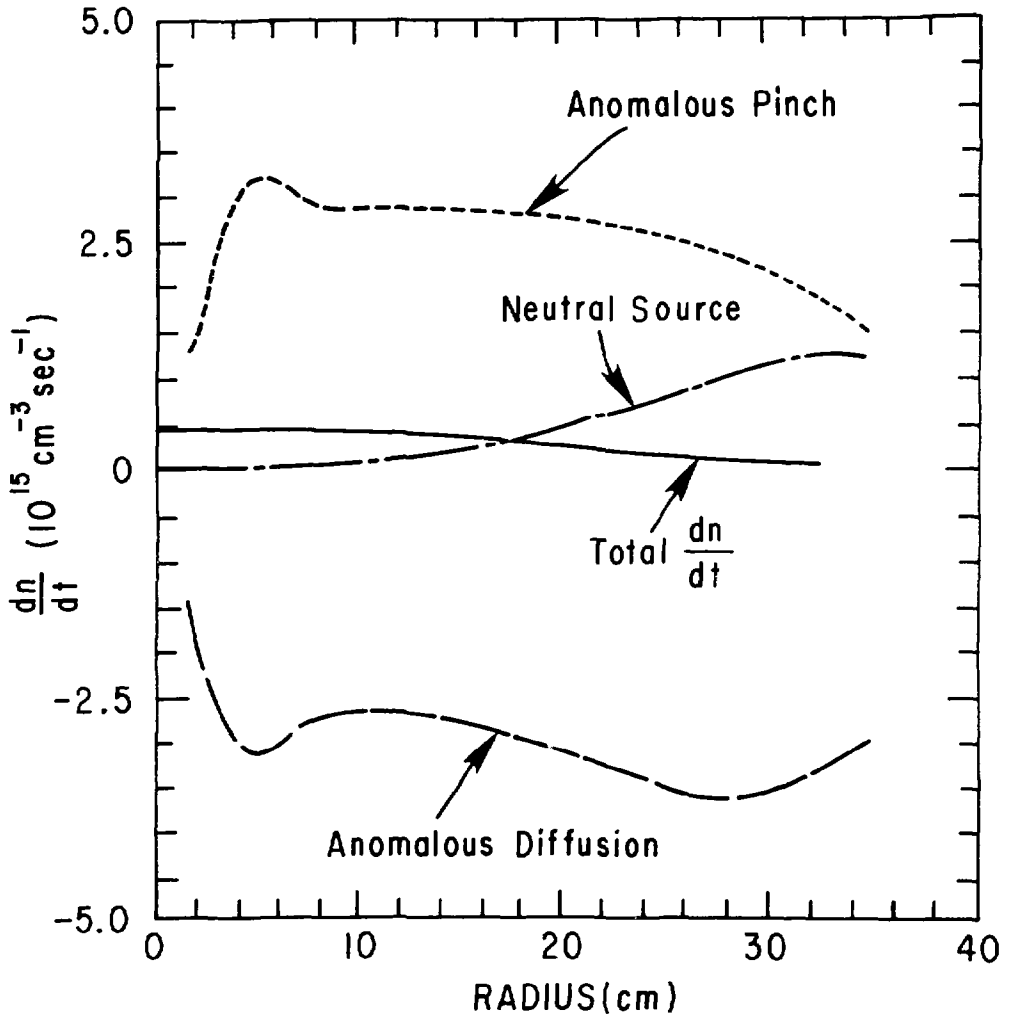


Fig. 18

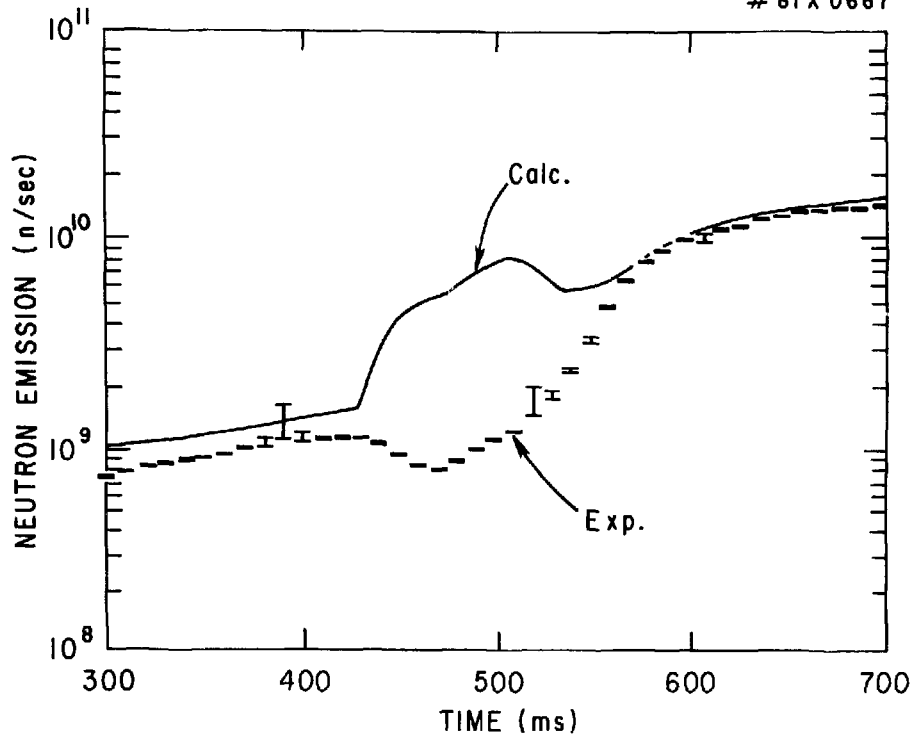


Fig. 19

82X0197

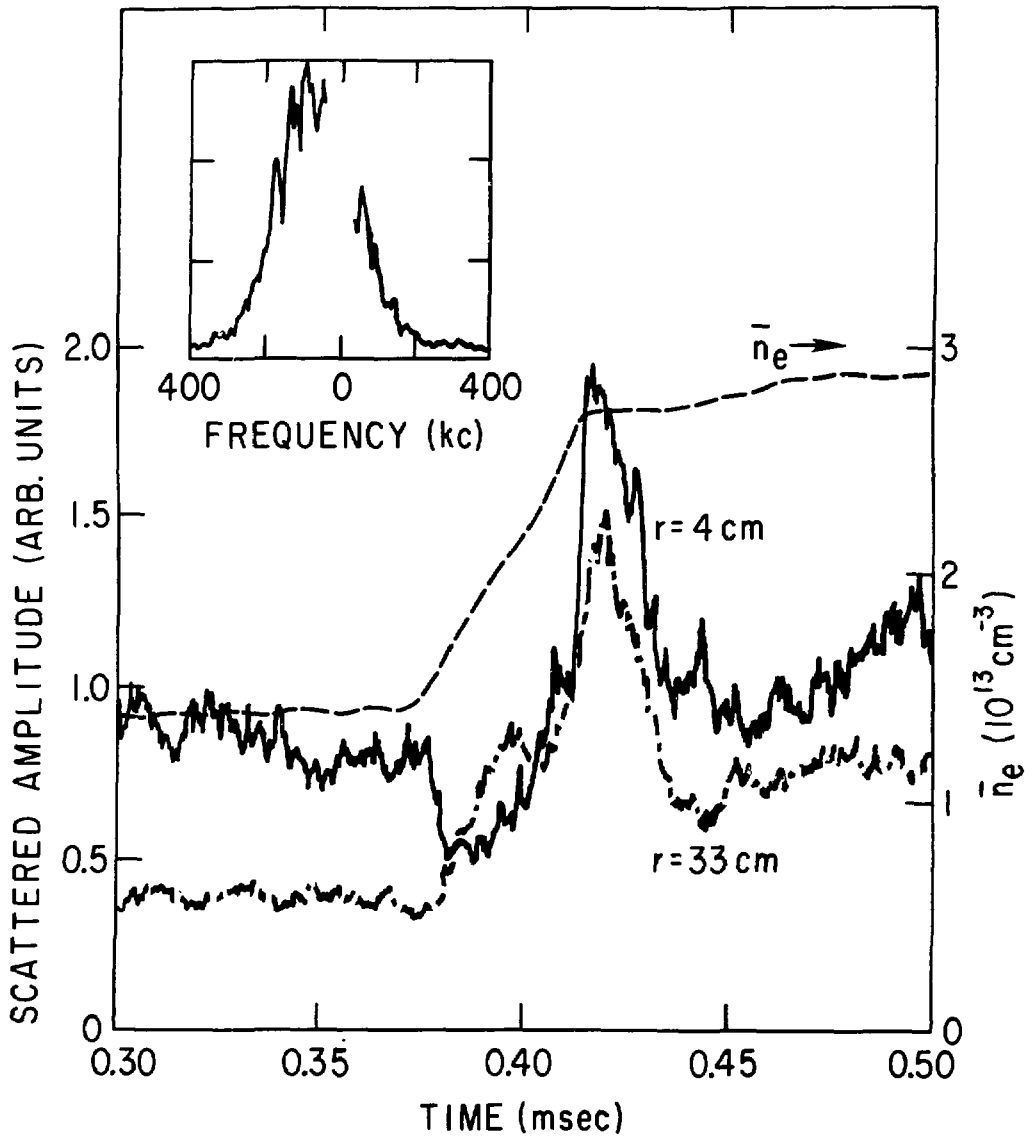


Fig. 20

81 X 0167

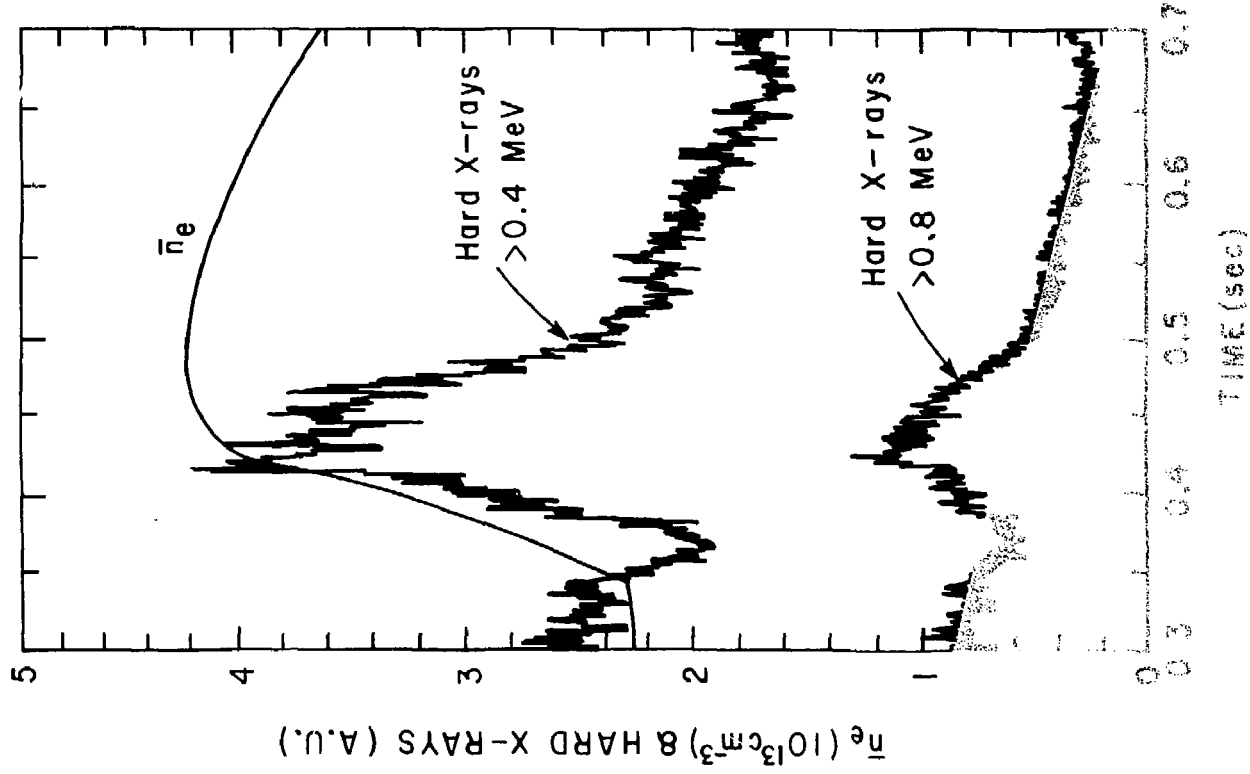


Fig. 3

81 X 0173

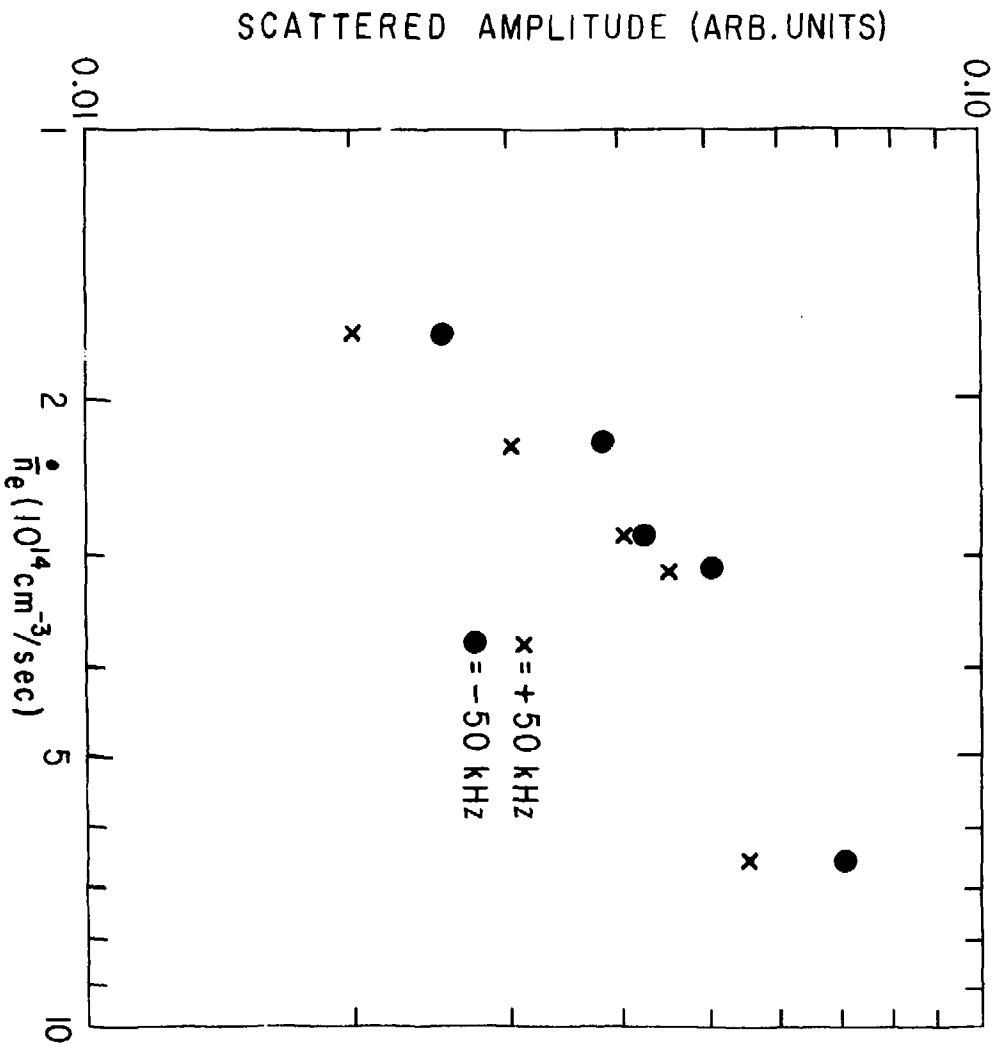


Fig. 22

82X0133

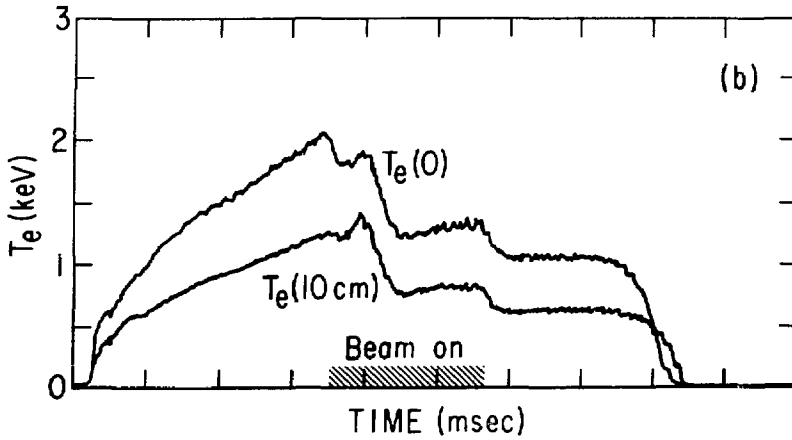
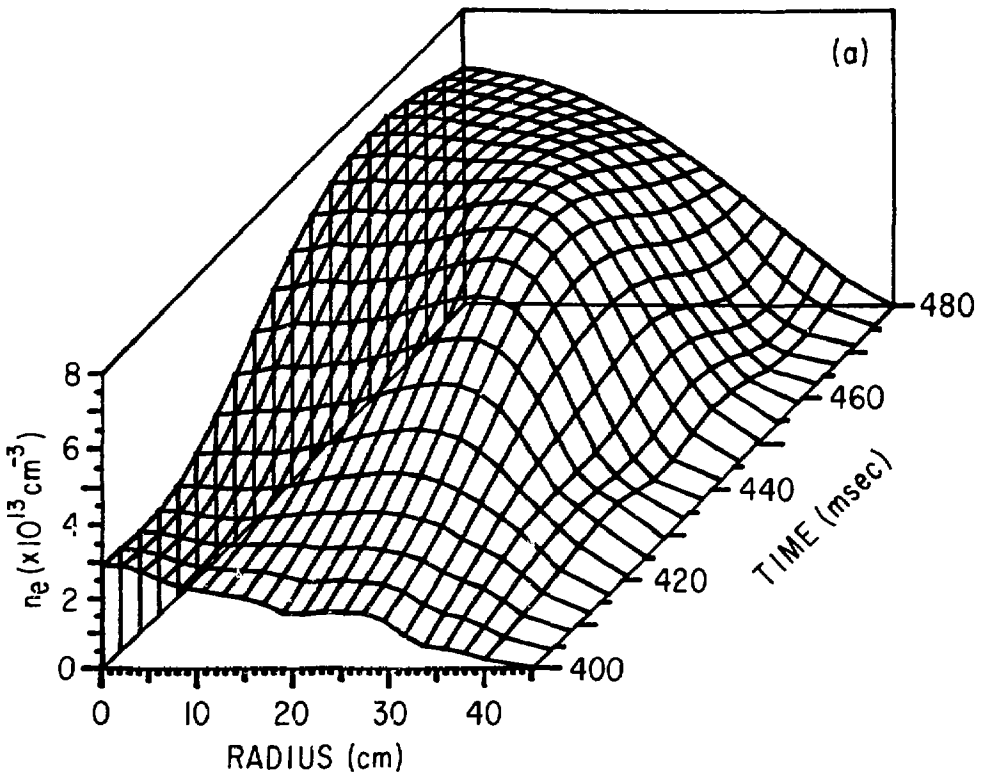


Fig. 23a,b

82X0127

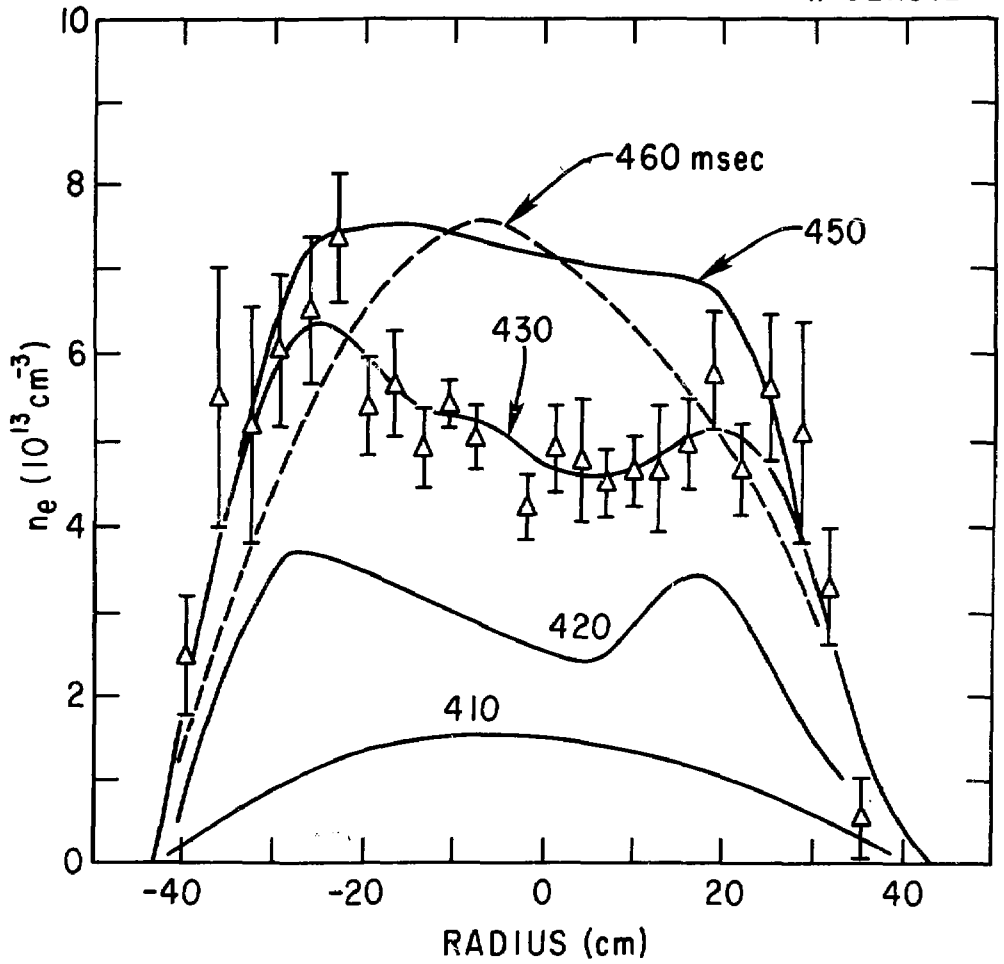


Fig. 23c

81 X 0169

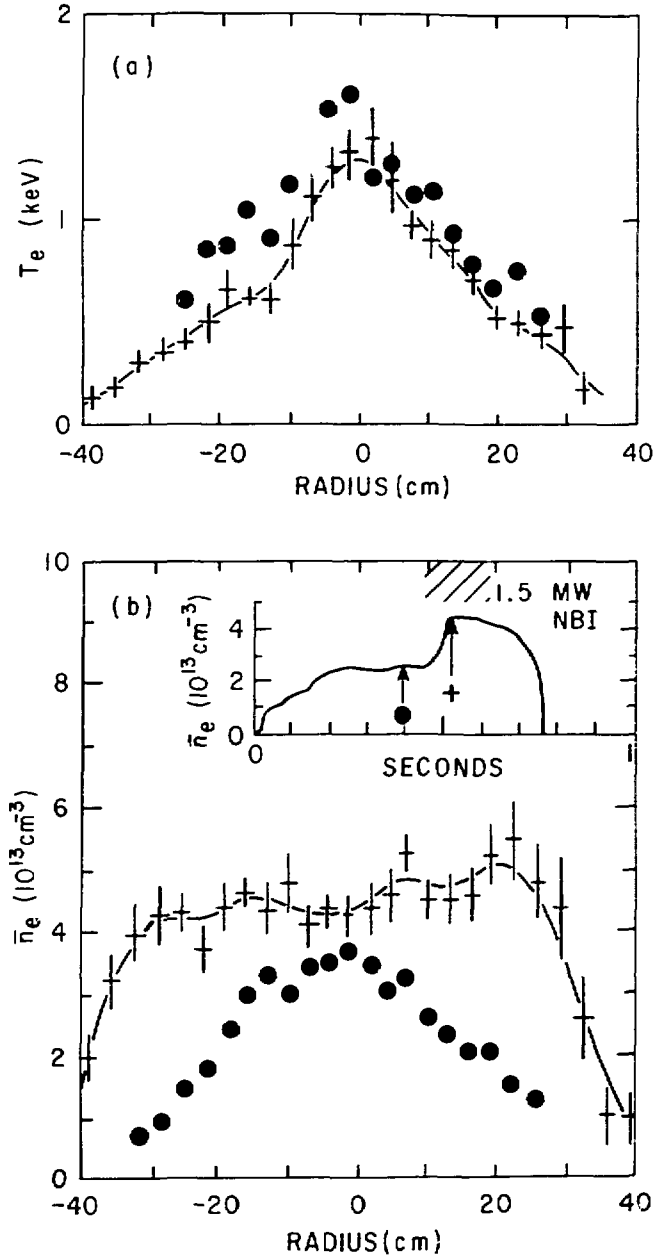


Fig. 24